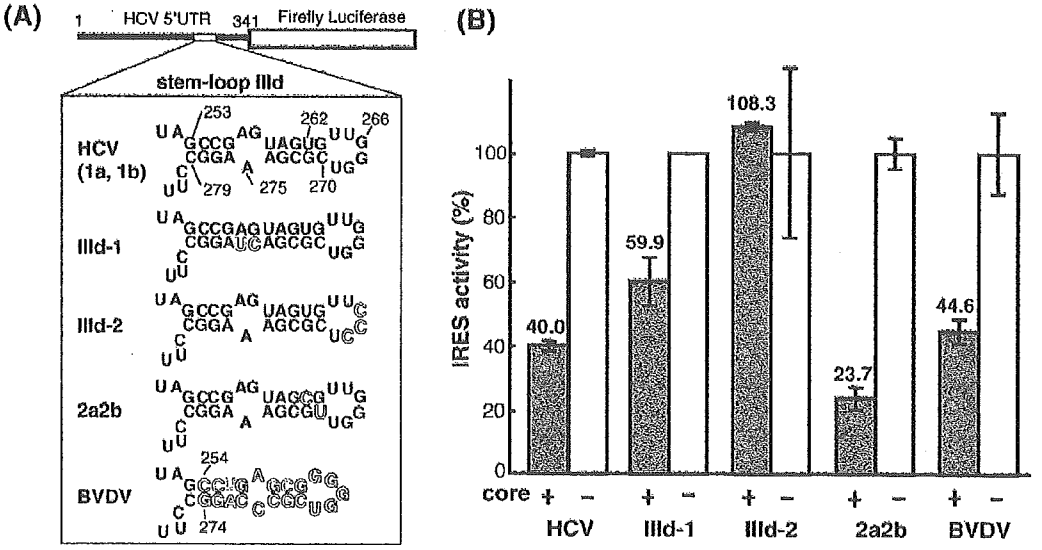

Fig. 4. Mutational analysis of the stem-loop IIId domain. (A) Schematic representation of the predicted secondary structures of the IIId domain of mutated reporters used in this study. (B) The core protein and luciferase reporters are expressed as described in the legend to Fig. 3, except reporters indicated. HCV IRES activity was determined and presented as described in the legend to Fig. 3C.

Mutational analysis of the stem-loop IIId domain

To further investigate the functional role of the stem-loop IIId domain (nt 253–279) in core protein-mediated inhibition of HCV translation, we engineered stem-loop IIId domains with the following four mutations (Fig. 4A): (1) IIId-1Luc, in which the A at nt 275 was changed to UC, thus forming a double-stranded structure instead of a bulge loop in the IIId, (2) IIId-2Luc, in which the GGG triplet (nt 266–268) was changed to a CCC triplet within the loop of stem-loop IIId, (3) 2a2bLuc, in which the U at nt 262 and the C at nt 270 were changed to C and U, respectively, thus changing the genotype to 2a/2b, and (4) BVDVLuc, in which the stem-loop IIId (nt 254–274) sequence was changed to that of bovine viral diarrhea virus (BVDV)-1. Cells that did or did not express the core protein were transfected with each of the above described reporter RNA transcripts, after which luciferase activity was measured. As shown in Fig. 4B, IIId-2Luc, containing a mutation of the GGG triplet of the apical loop, demonstrated no inhibition of HCV IRES-mediated translation by the core protein, whereas IIId-1Luc, containing a mutation within the bulge loop structure, showed only a marginally reduced inhibitory effect of the core protein. We previously demonstrated that HCV core protein binds most efficiently to (1) the stem-loop IIId domain, compared to other structural domains of the 5′UTR, and to (2) G octamer (G_8), as opposed to A_8, C_8, and U_8, using a quantitative SPR method (Tanaka et al., 2000). Thus, the results obtained here suggest that the apical loop is a critical recognition site for translational inhibition by the core protein. It is likely that the inhibitory activity of the core protein on HCV IRES-mediated translation is related to its efficiency of RNA binding.

We also observed the core protein to exert an inhibitory effect on translation directed by either 2a2bLuc or BVDVLuc, similar to that observed with wild-type HCVLuc, involving a 5′UTR sequence of genotype 1. Since the IIId domain sequence of HCVLuc is conserved among genotypes 1, 3, 4, and 5 and since that of 2a2bLuc is shared with genotype 6, it appears that inhibition of HCV translation by the core protein is independent of the viral genotype and occurs in most HCV isolates. Sequence alignment of HCV and various pestiviruses showed that, although the primary nucleotide sequence of the IIId domain exhibits considerable variability, the predicted secondary structure of the domain is highly conserved among these viruses as reviewed previously (Rijnbrand and Lemon, 1999). Furthermore, the GGG triplet followed by U at the apical loop and one bulge loop in the domain are well conserved among HCV and pestiviruses. These suggest that the nucleotide sequence of the apical loop, particularly the GGG triplet, is more important than the stem-structure sequence of the IIId domain for core protein-mediated translational inhibition.

Relationship between translational inhibition and ability of the core protein to bind to the IIId domain within the 5′ UTR

To investigate the relationship between inhibition of HCV translation by the core protein and ability of the core protein to bind to IIId RNA, we prepared two biotinylated oligo RNA molecules, IIId-1 and IIId-2 (nt 251–282), containing identical mutations in the bulge and apical loops of their IIId domains as the mutated reporters IIId-1Luc and IIId-2Luc, respectively (Fig. 4A). These mutant or wild-type oligo RNA (IIId-wt) molecules were then coupled to streptavidin-coated sensor chips and allowed to bind to purified recombinant core protein. The results of subsequent SPR analysis using a BIAcore biosensor are shown in Fig. 5. The core protein was observed to bind to IIId-1 RNA as efficiently as to IIId-wt RNA,

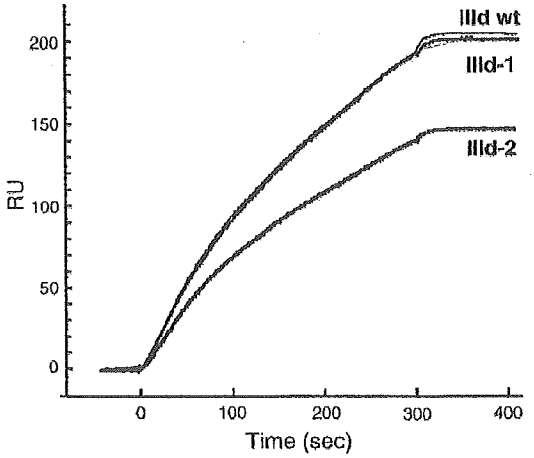

Fig. 5. Binding of the core protein to oligo RNAs corresponding to the mutated IIId domains. The real time binding between the core protein and wild-type (IIId wt) or mutants (IIId-1 and IIId-2) of the stem-loop IIId was examined. Biotinylated oligonucleotides were immobilized of the streptavidin pre-coated sensor chips followed by being exposed to 40 μl of the solution containing the core protein (4 μg/ml) with a flow rate of 8 μl/min. The sample flow was stopped, and the buffer washout began at 300 s. The amounts of immobilized synthetic oligonucleotides, IIId-wt, IIId-1, and IIId-2 were 211.0, 206.9, and 212.4 resonance units, respectively.

suggesting that RNA mutations disrupting the bulge loop structure have little or no effect on binding of the core protein. In contrast, a marked reduction in binding affinity of the core protein for mutant IIId-2 RNA was observed. As a negative control, we found that the core protein does not bind to oligo RNA corresponding to IIIe or IIIf domain (data not shown; Tanaka et al., 2000). It is likely that the apical loop sequence and/or the GGG triplet are important for RNA binding of the core protein, which is consistent with prior observations suggesting that the core protein binds to G-stretch sequence(s) with high affinity.

Combined with the data shown in Fig. 4B, the inhibitory effect of the core protein on HCV IRES activity correlates well with its ability to bind to wild-type and mutated IIId RNA. In light of the observation that the IIId domain is important for IRES activity and from suggestion that the domain IIId interacts with 40S (Otto et al., 2002; Jubin et al., 2000; Lukavsky et al., 2000; Spahn et al., 2001), the HCV core protein may inhibit viral IRES-dependent translation by preventing required interactions between RNA molecules and the 40S by binding to the IRES sequence including the apical loop of the IIId domain.

Role of basic-residue clusters within the core protein in inhibition of HCV translation

The amino-terminal portion of the core protein is able to bind to viral nucleic acids (Santolini et al., 1994). This region contains three clusters of arginine- and lysine-rich sequences (aa 5–13, 38–43, and 58–71). To investigate the role of these basic-residue clusters in inhibition of HCV translation by the core protein, we constructed a series of core mutants, in which lysine and arginine residues within one or more of the basic-residue clusters of the core protein were substituted with alanine residues, as depicted in Fig. 6A. Two days after transfection with either wild-type (pCAGC191) or core mutant (pCAGC191m1–m7) constructs, the cells were cotransfected with HCVLuc and capped-RLuc RNA. As indicated in Fig. 6B, core mutants containing alanine substitutions within one or two clusters (C191m1, m2, m3, m4, m5, and m6) retained the ability to inhibit HCV IRES-mediated translation, similar to the wild-type core protein. However, a core mutant with alanine substitutions involving all three clusters, C191m7, demonstrated little to no inhibition of translation. Expression of the core protein in each transfectant was determined by Western blotting (Fig. 6C), and none of the mutants influenced cap-dependent translation (data not shown). These results

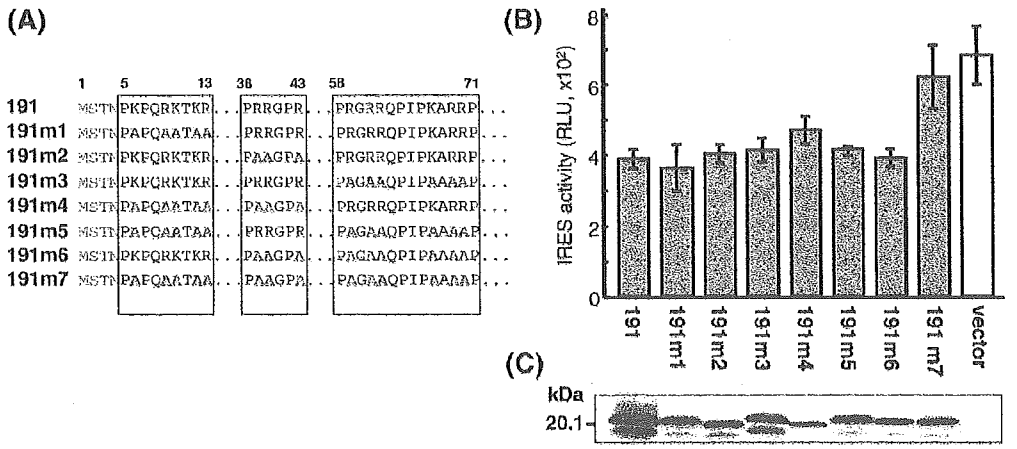

Fig. 6. A role of basic-residue clusters within the core protein in inhibition of the HCV translation. (A) Schematic representation of the mutated core proteins substituted in three basic aa clusters. Lysine or arginine residues substituted with alanine in the clusters are shown with outlined letters. (B) Two days after the transfection with either wild-type (191) or mutated (191m1–m7) core-expressing constructs, HepG2 cells were further cotransfected with HCVLuc and capped-RLuc RNAs. Relative luciferase activities (RLU) were determined as described in Materials and methods and the legend to Fig. 3. (C) The amounts of the wild-type and mutant core proteins expressed in HepG2 cells are shown by Western blotting.

suggest that all three basic-residue clusters of the core protein can mediate inhibition of HCV translation and that at least one cluster is required for inhibition.

Discussion

In this study, we investigated the mechanism by which the core protein modulates HCV IRES activity using an in vivo reporter assay and SPR technology. We demonstrated the importance of a stem-loop IIId domain, spanning nt 253–279, in core protein-mediated inhibition of HCV IRES-mediated translation. In a previous study, we demonstrated preferential binding of the core protein to domain IIId of the 5′UTR followed by domain I and a region spanning nt 23–41 (Fig. 1), upon examining 10 oligonucleotides corresponding to various structured domains of the viral 5′UTR (Tanaka et al., 2000). The core protein did not have an inhibitory effect on translation directed by mutated IRES lacking the IIId domain. However, translation initiated by IRES mutants with deletions of domain I or nt 23–41 was significantly inhibited by the core protein to a similar extent as wild-type IRES-mediated translation (Fig. 3B). Further mutational analysis was then used to determine whether specific IIId nucleotide sequences were important for inhibition of translation by the core protein. We determined that the GGG triplet (nt 266–268) within the IIId apical loop was most critical for core protein-mediated inhibition (Fig. 4B). Combined with the results of SPR analysis (Fig. 5), the data presented here suggest that inhibition of HCV IRES-directed translation by the core protein depends on the binding efficiency of the core protein for the viral IRES element.

Domain III, which is composed of six distinct regions containing stem-loop structures, forms the core of the HCV IRES and is essential for viral translation. Previous studies suggest that domain III plays a role in recruiting the 40S ribosomal subunit and eIF3 by direct interaction with stem-loops IIId/e/f and IIIb, respectively, even though the 40S subunit makes multiple interactions with the IRES and also binds to stem-loop II and the pseudoknot domain of the IRES element (Kieft et al., 2001; Kolupaeva et al., 2000; Sizova et al., 1998). Stem-loop IIId is a highly conserved region within domain III in most HCV isolates, consisting of two double-stranded helical elements separated by a 3-nt internal asymmetric loop with a 6-nt hairpin loop at the distal end of each helical region. IRES sequence deletions, including deletion of stem-loop IIId, as well as point mutations, inhibit binding of the 40S subunit and IRES function (Rijnbrand et al., 1995; Honda et al., 1996; Kieft et al., 1999). Specifically, substitution mutations of the GGG triplet within the IIId apical loop region produce significant loss of IRES activity, as well as alterations in RNA folding, indicating that the GGG triplet is a critical region for HCV translation (Kieft et al., 1999; Jubin et al., 2000). In addition, antisense 2′-*O*-methyloligonucleotides targeted to the IIId domain are known to compete with the 40S subunit for binding and to inhibit viral translation (Tallet-Lopez et al., 2003). Moreover, the secondary structure of the IIId domain is important for binding of the S9 ribosomal protein (Odreman-Macchioli et al., 2000). Consistent with these observations, we also observed that deletion of the IIId domain (ΔIIIdLuc), or a G-to-C substitution within the GGG triplet (IIId-2Luc), significantly reduced IRES activity.

Although the sequence of the IIId domain is highly conserved, sequence polymorphism of the helical region exists among the six major genotypes. With regard to nt 262 and nt 270 of the IIId domain, genotypes 1, 3, 4, and 5 of HCV encode U (nt 262) and C (nt 270), respectively. On the other hand, genotypes 2 and 6 encode C (nt 262) and U (nt 270), respectively. We observed that translation directed by the IRES sequence of genotypes 2 and 6 (2a2bLuc) was more efficient than that directed by the IRES sequence of genotypes 1, 3, 4, and 5 (HCVLuc) (Fig. 4B). Previous studies also demonstrated differences in the efficiency of IRES activity among different HCV genotypes and suggest that the 5′UTR of genotype 2(b) has the most marked IRES activity (Tsukiyama-Kohara et al., 1992; Kamoshita et al., 1997; Collier et al., 1998). Thus, sequence polymorphism involving the helical region of IIId might explain the observed variability in IRES activity when comparing the 5′UTR sequences of different HCV genotypes. Expression of the core protein inhibits HCV translation directed by 2a2bLuc to a similar or same extent as that directed by HCVLuc. This finding suggests that inhibition of viral translation by the core protein commonly occurs during the HCV life cycle and is not limited to certain genotypes. The deletion of the 5′-proximal stem-loop domain I (ΔILuc) significantly reduced IRES activity (data not shown), although the ability of the core protein to inhibit translation was retained (Fig. 3B). Published data regarding the role of domain I in inhibition of HCV translation are not consistent. Some researchers suggest that the 5′-proximal region containing domain I is not essential for HCV IRES activity (Honda et al., 1996; Kamoshita et al., 1997). However, other researchers suggest that this stem-loop element is required for optimal IRES-mediated HCV translation (Friebe et al., 2001; Fukushi et al., 1994; Luo et al., 2003). We compared HCV IRES activity mediated by monocistronic and bicistronic reporters with deletion of domain I and found that an inhibitory effect of the domain I deletion observed from the bicistronic reporter was less evident than that from the monocistronic one: the reduction in IRES activity caused by the deletion was 95% and 40% for the monocistronic and bicistronic constructs, respectively. Although similar trends were observed in the previous studies using cultured cells (Friebe et al., 2001; Luo et al., 2003; Kamoshita et al., 1997), in vitro transcription/translation studies demonstrated that the translational efficiency of the reporters deleted with domain I is higher than that of the wild-type (Honda et al., 1996; Kamoshita et al., 1997). It may be likely that differences in (1) gene constructs such as monocistronic and bicistronic reporters and (2) host cell conditions influence such inconsistent observations.

HCV core protein is highly basic, especially its N-terminal half, and it is thought to encapsulate the viral genome within a viral nucleocapsid. The RNA-binding domain of the core protein has been mapped to 75 aa residues within the N-terminal, in which three clusters of highly arginine/lysine-rich sequences are well conserved among HCV isolates (Santolini et

al., 1994). We previously observed preferential binding between the core protein and positive-stranded HCV RNA spanning the 5′UTR and part of the structural-protein coding region (nt 1–2327) (Shimoike et al., 1999). In this study, we demonstrated the importance of three basic aa residue clusters within the N-terminal region of the HCV core protein for its inhibitory effect on viral IRES activity. At least one cluster is required for inhibition of translation by the core protein. Previous studies with a series of deletion mutants suggest that aa 34–44 (Zhang et al., 2002) or aa 1–20 (Li et al., 2003) within the core protein are crucial for inhibition of translation initiated by HCV IRES. To investigate the contribution of these basic-residue-rich domains within the core protein to inhibition of viral translation, we employed substitution mutagenesis of the full-length core protein in order to reduce the occurrence of conformational changes in the core protein due to the introduction of mutations.

Although an increasing body of evidence shows involvement of the core protein in translational regulation, there are conflicting data regarding the exact mechanism by which this occurs. In contrast to studies describing direct inhibition of HCV translation by expression of the core protein (Shimoike et al., 1999; Zhang et al., 2002; Li et al., 2003), a recent report suggests that the core protein modulates HCV IRES function in a dose-dependent manner, with low amounts of the core protein producing up-regulation and greater amounts resulting in down-regulation (Boni et al., 2005). The core protein does not only inhibit translation initiated by the HCV IRES, but also cap-dependent translation and translation initiated by encephalomyocarditis virus (EMCV) IRES (Li et al., 2003). In an earlier study, neither cap- nor EMCV IRES-dependent translation were inhibited by expression of the core protein (Shimoike et al., 1999). Other studies suggest that the core protein-coding sequence, but not the core protein itself, modulates HCV IRES function, through a long-range RNA–RNA interaction (Wang et al., 2000; Kim et al., 2003). In the present experiment, however, down-regulation of HCV IRES-directed translation by the core protein-coding RNA sequences was eliminated by introducing a base-substitution mutation into the N-terminus of the core sequence in order to create a termination codon (Fig. 2). These contradictory findings might be due to different experimental conditions, such as the use of different reporter systems and host cells, as well as different levels of core protein in the assays used. To investigate the effect of the core protein on HCV IRES-dependent translation, we employed in vivo RNA transfection of monocistronic reporter constructs because HCV IRES is located at the 5′ end of the viral genome, and not internally, thus making it unnecessary to use a bicistronic reporter. Concerning bicistronic contexts, the possibility that the first cistronic sequence might influence IRES regulation directed by the second cistronic gene cannot be excluded. There is evidence to suggest that differences in translational regulation by the core protein might exist among different cell lines, including HepG2, Huh-7, and CV-1 cells (Wang et al., 2000; Li et al., 2003). We also observed differences between HepG2 and Huh-7 cells in terms of ability of the core protein to inhibit HCV IRES- and cap-dependent translation, which was not observed in Huh-7 cells (data not shown), as previously reported (Wang et al., 2000). Such cell-type specific effects might be related to differences in core protein expression since core protein expression by the recombinant baculovirus AcCA39 seems to be less abundant in Huh-7 cells, compared to HepG2 cells (data not shown). It is also possible that a cell-specific factor(s) are involved in translational regulation by the core protein. Thus, some interaction(s) between the highly ordered HCV IRES structure and/or the core protein and related host factors are likely cell-type-specific. Our previous report showed difference in the translation efficiency mediated by HCV IRES among human liver-derived cell lines, although the effect of the core protein on their translation was not determined (Aoki et al., 1998).

We performed the gel mobility shift assay to demonstrate the inhibition of the interaction between the HCV 5′UTR and the ribosome 40S subunit (40S). The complexes between purified 40S and the radiolabeled HCV 5′UTR (nt 1–330) were detected, and the amount of this band was decreased in the core protein-dose-dependent manner. In this condition, the core–5′UTR complex was competed with a non-labeled oligo RNA corresponding to IIId domain, but not with oligo RNAs of domain IV. However, the complex between the core protein and the 5′UTR was detected around the wells of the gel. To our knowledge, there has been no published data that in the gel mobility shift assay the core–5′UTR complex runs into the gel. Although these findings may support the idea that the core protein directly prevents binding of 40S to the HCV IRES, direct biochemical probing of the proposed interaction must wait for the advances in the protein chemistry of the HCV core protein.

Finally, based on the results of the present study and the existing literature, we propose a model of down-regulation of HCV translation mediated by the core protein (Fig. 7). In HCV-infected cells, the virus uncoats and releases its genomic RNA, which serves as a template for protein translation. Highly folded secondary and tertiary RNA elements in the 5′UTR function as *cis* signals for interaction with the 40S subunit and eIF3 during the initial process of HCV IRES-dependent translation. The high affinity interaction between HCV IRES and the 40S subunit is thought to be important for recruitment of the 43S particle to viral RNA, and the stem-loop IIId domain is a prerequisite for this interaction. Since the core protein binds most efficiently to the IIId domain in the HCV IRES element, it is relevant to note that the core protein may prevent an essential RNA–40S interaction by blocking the IIId domain, thereby reducing the viral translation efficiency. At an early stage of the HCV replication cycle, translation of the viral genome yields a polyprotein, which is subsequently processed to yield individual mature proteins. At a certain point, enough core protein is available to inhibit HCV translation by competing with the 40S subunit for IRES binding. Cells in which HCV translation is negatively controlled may have reduced levels of core protein due to its degradation by the ubiquitin/proteasome pathway (Suzuki et al., 2001; Moriishi et al., 2003), thereby decreasing the inhibitory effect of core protein. Thus, the core protein may

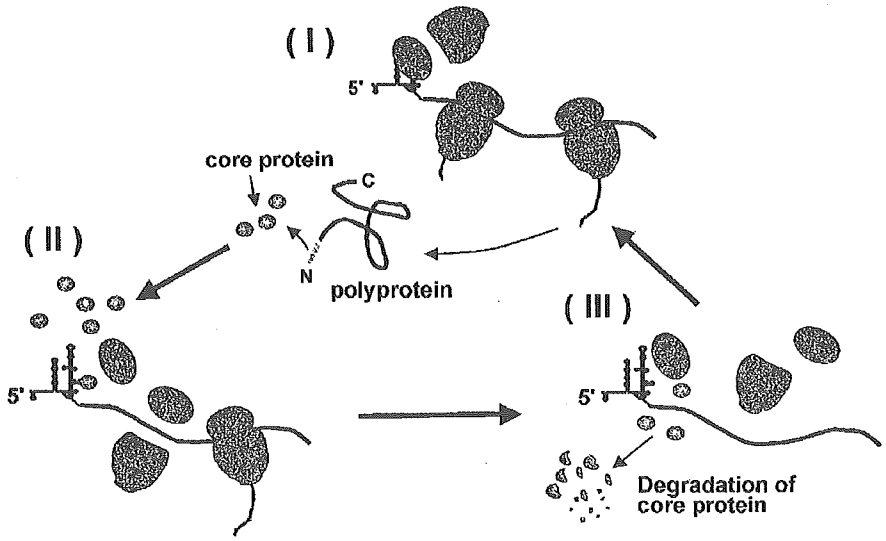

Fig. 7. Model for the regulation of HCV translation mediated by the core protein. Step 1: HCV translation is initiated through recognition of the 40S subunit and eIF3 by the IRES RNA tertiary structure. The viral polyprotein is expressed and processed into matured proteins, resulting in generation of the core protein. Step 2: The expressed core protein binds to the stem-loop IIId in the 5′UTR and inhibits the viral translation by competing with 40S subunit for binding to the IRES. Step 3: The reduced translational efficiency results in decreasing the levels of HCV proteins and replication. Degradation of the core protein through the ubiquitin/proteasome pathway may also contribute to reducing the amounts of the core protein in cells. A low concentration of the core protein possibly leads to recovery of the translational efficiency.

contribute, through its competitive interaction with the IRES IIId domain, to virus persistence by maintaining a low level of HCV replication.

Materials and methods

Plasmid construction

pT7ΔloopILuc (termed ΔILuc in this report), a 271-nt fragment containing a T7 promoter followed by nt 23–249 from the 5′ terminus of the HCV genome (clone NIHJ1; genotype 1b) (Aizaki et al., 1998), was amplified by PCR using pT7HCVLuc (HCVLuc) (Shimoike et al., 1999) as a template and primers *Hin*dIIIT7S (5′-CCCAAGCTTTAATACGACTCACTATACACTCCACCATAG-3′) and *Nhe*IAS (5′-CTAGCTAGCAGTCTCGCGCGGGG-3′). The PCR product was digested with both *Hin*dIII and *Nhe*I and ligated with a 5.3-kbp *Hin*dIII–*Nhe*I fragment of pT7HCVLuc. pT7Δ23–41Luc (Δ23–41Luc) was made using a QuickChange Site-Directed Mutagenesis Kit (Stratagene, La Jolla, CA) in order to introduce a deletion of nt 23–41 from the 5′ terminus. The primers used for PCR were 23–41S (5′-CCTAGATTGGGGGCGACCCCTGTGAGGAAC-3′) and the 23–41 AS complement (5′-GTTCCTCACAGGGGTCGCCCCCAATCAGG-3′), and pT7HCVLuc was used as a template.

pT7ΔIIIdLuc (ΔIIIdLuc) was made by digestion of pT7HCVLuc with *Nhe*I and *Stu*I, thereby generating 30-bp (corresponding to the stem-loop IIId region), 1.8-kbp, and 3.8-kbp fragments. After this, the 1.8-kbp and 3.8-kbp fragments were isolated, blunt-ended, and then ligated.

pT72a2bLuc (2a2bLuc), pT7BVDVLuc (BVDVLuc), pT7IIId-1Luc (IIId-1Luc), and pT7IIId-2Luc (IIId-2Luc) were made as follows. pT7HCVLuc was partially digested with *Stu*I. A 5.6-kbp fragment was isolated and completely digested with *Nhe*I. The resulting fragment was ligated with annealed two partially complementary oligonucleotides with the following *Nhe*I and *Stu*I sites: 5′-CTAGCCGAGTAGTGTTGGGTCGCGACTAGG-3′ and 5′-CCTAGTCGCGACCCAACACTACTCGG-3′ for IIId-1,5′-CTAGCCGAGTAGTGTTCCCTCGCGAAAGG-3′ and 5′-CCTTTCGCGAGGGAACACTACTCGG-3′ for IIId-2, 5′-CTAGCCGAGTAGCGTTGGGTTGCGAAAGG-3′ and 5′-CCTTTCGCAACCCAACGCTACTCGG-3′ for 2a2b, and 5′-CTAGCCTGAGCGGGGGTCGCCCAGG-3′ and 5′-CCTGGGCGACCCCCGCTCAGG-3′ for BVDVLuc (the underlined nucleotides were substituted for the wild type nucleotides; see Fig. 4A).

pRLucHCVLuc, pRLucΔ23–41Luc, and pRLucΔIIIdLuc: 2.6-kb fragments were amplified by PCR using pT7HCVLuc, pT7Δ23–41Luc, and pT7ΔIIIdLuc as template DNAs, respectively, and primers *Xba*I 5′endS (5′-GCTCTAGAGCCAGCCCCCGATTGGGGGCGA) and *Xba*I 3′endAS (5′-GCTCTAGAACTAGTGGATCCGGAT). The PCR products were digested with *Xba*I and ligated with a 3.3-kb *Xba*I fragment of pRL-null Vector (Promega, Madison, WI).

pRLucΔILuc: 2.6-kb fragment was amplified by PCR using pT7ΔILuc as a template DNA and primers *Xba*IloopIS (5′-GCTCTAGACACTCCACCATAGATCACCCCC) and *Xba*I 3′endAS. The PCR product was digested with *Xba*I and ligated with a 3.3-kb *Xba*I fragment of pRL-null Vector.

pCAGC191 (Suzuki et al., 2001) carries nt 329–914, containing the entire HCV coding region of the core protein of clone HCV J1 (Aizaki et al., 1998), controlled by the CAG promoter. pCAGFS contains a frame shift mutation, involving substitution of A with T at nt 357, to make a stop codon (TAA)

(refer to Fig. 1). Only the first five residues (MSTNP) of the core protein are translated from this plasmid. To create a series of mutated core-expressing constructs: pCAGC191m1, -m2, -m3, -m4, -m5, -m6, and -m7, alanine substitutions were introduced into the basic-residue clusters of the core protein by PCR mutagenesis with primers containing base alterations, as described previously (Suzuki et al., 2005). The PCR products were then cloned into pCR2.1 (Invitrogen Corp., Carlsbad, CA) and verified by DNA sequencing. Individual cDNAs were excised and inserted separately into pCAGGS. The primer sequences used in these constructions are available from the authors upon request.

Cells

A human hepatocellular carcinoma cell line, HepG2, was obtained from the American Type Culture Collection. Cells were maintained in Dulbecco's modified Eagle's medium (Nissui, Tokyo, Japan) containing 50 μg/ml of Gentamycin (Biological Industries Ltd., Israel) and supplemented with 10% fetal calf serum.

RNA preparation

The reporter plasmids were linearized by digestion with adequate restriction enzymes, and the resulting DNA fragments were used as templates for in vitro transcription. HCVLuc and a series of HCVLuc mutants were linearized by digestion with *Xho*I. pRL-null (Promega, Madison WI) was linearized by *Xba*I digestion. pRLucHCVLuc and a series of pRLucHCVLuc mutants were linearized by *Bam*HI digestion. An in vitro transcription kit, MEGAscript (Ambion, Austin, TX), was used for RNA synthesis, during which reaction mixtures containing 1 μg of DNA template and 2 μl of T7 enzyme mix were incubated at 37 °C for 2 h. For capped RNA synthesis, linearized pRL-null, pRLucHCVLuc, and a series of pRLucHCVLuc mutants were used as templates, and 2 μl of each ATP, CTP, and UTP (7.5 mM), as well as 1 μl of GTP (7.5 mM) and 1 μl of cap homologue m7G (5′) ppp (5′) G (7.5 mM; Ambion), was used. The reaction mixtures were subsequently treated twice with 2 U of DNase I at 37 °C for 20 min followed by EDTA (25 mM) and lithium chloride (3.75 M) to terminate the reaction. Capped mRNA synthesized contained 11 nucleotides at 5′UTR and no poly(A) tail.

Transfection

For DNA transfection, 100 μl of Opti-MEM (Invitrogen Corp.) and 4 μl of TransIT-LT1 reagent (Mirus Corp., WI) were mixed and incubated at room temperature for 5 min followed by the addition of 2 μg of each plasmid expressing core protein, mutant core protein, or empty vector followed by incubation for a further 15 min. For RNA transfection, synthesized reporter RNA and 2.5 μl of Tfx-20 (Promega) were mixed in 100 μl of Opti-MEM and incubated for 15 min prior to transfection. One day prior to DNA transfection, cells (2.5×10^5) were seeded into a 12-well plate. The transfection mixture described above was added to the cells in 500 μl of Opti-MEM medium after the cells were washed twice with 500 μl of Opti-MEM.

Luciferase assay

The cells infected or transfected with a recombinant baculovirus or plasmid carrying the entire HCV core gene (AcCA39 or pCAGC191) or an empty vector (AcCAG or pCAGGS) were cultured for 2 days followed by transfection with reporter RNA, either HCVLuc (0.1 μg/well), ΔILuc (6.0 μg/well), Δ23–41Luc (0.2 μg/well), ΔIIIdLuc (6.0 μg/well), IIId-1 (0.1 μg/well), IIId-2 (6.0 μg/well), 2a2bLuc (0.1 μg/well), or BVDVLuc (0.1 μg/well), along with capped RL RNA (0.08 μg/well). After 6 h of incubation, FL and RL activities were determined using the Dual-Luciferase Reporter Assay System (Promega), as previously described (Aoki et al., 1998; Shimoike et al., 1999). Luminescent signals were measured with a TR717 luminometer (Applied Biosystems Japan Ltd., Tokyo, Japan).

Western blot analysis

Expression of HCV core protein was detected by Western blotting, as previously described (Shimoike et al., 1999). Briefly, protein was transferred to a polyvinylidene difluoride (PVDF) membrane (Immobilon; Millipore, Tokyo, Japan) after separation by SDS-PAGE. After blocking, the membranes were probed with a polyclonal antibody against glutathione-*S*-transferase core (aa 1–191) fusion protein, at a 1:100 dilution.

SPR experimental procedure

To prepare the core protein, insect Tn5 cells were infected with a recombinant baculovirus Ac39. The core protein was partially purified from the cell lysate, as previously described (Tanaka et al., 2000). Interactions between the core protein and synthetic RNA oligonucleotides were examined by SPR analyses with BIAcore 2000 (Biacore K.K., Tokyo, Japan). The SPR experimental procedure was as previously described (Tanaka et al., 2000). Briefly, a biotinylated oligonucleotide spanning nt 251–282 (IIId-wt) and mutant IIId domains (IIId-1 and IIId-2) (Fig. 4A) were synthesized followed by immobilization on streptavidin pre-coated sensor chips. Forty microliters of solution containing the core protein (4 μg/ml) was injected onto the sensor chip surface at a flow rate of 8 μl/min. The sample flow was stopped, and buffer washout started at 5 min post-injection.

Acknowledgments

We are grateful to Professor J.D. Puglisi for helpful discussion. We would like to thank Drs. M. Tashiro, T. Yoneyama, H. Tani, H. Aizaki, K, and A. Cahour for helpful discussion. We are grateful to Drs. H. Tani and A. Rikimaru for constructing the recombinant baculoviruses and plasmids. We would also like to thank Ms. S. Ogawa, M. Matsuda, M.

Yahata, Y. Hirama, and T. Mizoguchi for their technical assistance and secretarial work.

This work was supported by JSPS.KAKENHI (13670309) and by a grant provided by the Ichiro Kanehara Foundation to T. Shimoike. This work was also supported in part by Research on Health Sciences focusing on Drug Innovation from the Japan Health Sciences Foundation; by grants-in-aid from the Ministry of Health, Labor and Welfare; and by the program for Promotion of Fundamental Studies in Health Sciences of the National Institute of Biomedical Innovation (NIBIO), Japan.

References

Aizaki, H., Aoki, Y., Harada, T., Ishii, K., Suzuki, T., Nagamori, S., Toda, G., Matsuura, Y., Miyamura, T., 1998. Full-length complementary DNA of hepatitis C virus genome from an infectious blood sample. Hepatology 27, 621–627.

Ali, N., Siddiqui, A., 1995. Interaction of polypyrimidine tract-binding protein with the 5′ noncoding region of the hepatitis C virus RNA genome and its functional requirement in internal initiation of translation. J. Virol. 69, 6367–6375.

Ali, N., Siddiqui, A., 1997. The La antigen binds 5′ noncoding region of the hepatitis C virus RNA in the context of the initiator AUG codon and stimulates internal ribosome entry site-mediated translation. Proc. Natl. Acad. Sci. U.S.A. 94, 2249–2254.

Ali, N., Pruijn, G.J., Kenan, D.J., Keene, J.D., Siddiqui, A., 2000. Human La antigen is required for the hepatitis C virus internal ribosome entry site-mediated translation. J. Biol. Chem. 275, 27531–27540.

Alter, H.J., Seeff, L.B., 2000. Recovery, persistence, and sequelae in hepatitis C virus infection: a perspective on long-term outcome. Semin. Liver Dis. 20, 17–35.

Aoki, Y., Aizaki, H., Shimoike, T., Tani, H., Ishii, K., Saito, I., Matsuura, Y., Miyamura, T., 1998. A human liver cell line exhibits efficient translation of HCV RNAs produced by a recombinant adenovirus expressing T7 RNA polymerase. Virology 250, 140–150.

Anwar, A., Ali, N., Tanveer, R., Siddiqui, A., 2000. Demonstration of functional requirement of polypyrimidine tract-binding protein by SELEX RNA during hepatitis C virus internal ribosome entry site-mediated translation initiation. J. Biol. Chem. 275, 34231–34235.

Boni, S., Lavergne, J.P., Boulant, S., Cahour, A., 2005. Hepatitis C virus core protein acts as a *trans*-modulating factor on internal translation initiation of the viral RNA. J. Biol. Chem. 280, 17737–17748.

Brown, E.A., Zhang, H., Ping, L.H., Lemon, S.M., 1992. Secondary structure of the 5′ nontranslated regions of hepatitis C virus and pestivirus genomic RNAs. Nucleic Acids Res. 20, 5041–5045.

Buratti, E., Tisminetzky, S., Zotti, M., Baralle, F.E., 1998. Functional analysis of the interaction between HCV 5′UTR and putative subunits of eukaryotic translation initiation factor eIF3. Nucleic Acids Res. 26, 3179–3187.

Choo, Q.-L., Richman, K.H., Han, J.H., Berger, K., Lee, C., Dong, C., Gallegos, C., Coit, D., Medina-Selby, A., Barr, P.J., Weiner, A.J., Bradley, D.W., Kuo, G., Houghton, M., 1991. Genetic organization and diversity of the hepatitis C virus. Proc. Natl. Acad. Sci. U.S.A. 88, 2451–2455.

Collier, A.J., Tang, S., Elliott, R.M., 1998. Translation efficiencies of the 5′ untranslated region from representatives of the six major genotypes of hepatitis C virus using a novel bicistronic reporter assay system. J. Gen. Virol. 79, 2359–2366.

Fan, Z., Yang, Q.R., Twu, J.S., Sherker, A.H., 1999. Specific in vitro association between the hepatitis C viral genome and core protein. J. Med. Virol. 59, 131–134.

Friebe, P., Lohmann, V., Krieger, N., Bartenschlager, R., 2001. Sequences in the 5′ nontranslated region of hepatitis C virus required for RNA replication. J. Virol. 75, 12047–12057.

Fukushi, S., Katayama, K., Kurihara, C., Ishiyama, N., Hoshino, F.B., Ando, T., Oya, A., 1994. Complete 5′ noncoding region is necessary for the efficient internal initiation of hepatitis C virus RNA. Biochem. Biophys. Res. Commun. 199, 425–432.

Fukushi, S., Okada, M., Kageyama, T., Hoshino, F.B., Nagai, K., Katayama, K., 2001. Interaction of poly(rC)-binding protein 2 with the 5′-terminal stem loop of the hepatitis C-virus genome. Virus Res. 73, 67–79.

Grakoui, A., McCourt, D.W., Wychowski, C., Feinstone, S.M., Rice, C.M., 1993. Characterization of the hepatitis C virus-encoded serine proteinase: determination of proteinase-dependent polyprotein cleavage sites. J. Virol. 67, 2832–2843.

Hahm, B., Kim, Y.K., Kim, J.H., Kim, T.Y., Jang, S.K., 1998. Heterogeneous nuclear ribonucleoprotein L interacts with the 3′ border of the internal ribosomal entry site of hepatitis C virus. J. Virol. 72, 8782–8788.

Hellen, C.U., Pestova, T.V., 1999. Translation of hepatitis C virus RNA. J. Viral Hepatitis 6, 79–87.

Hijikata, M., Kato, N., Ootsuyama, Y., Nakagawa, M., Shimotohno, K., 1991. Gene mapping of the putative structural region of the hepatitis C virus genome by in vitro processing analysis. Proc. Natl. Acad. Sci. U.S.A. 88, 5547–5551.

Honda, M., Ping, L.H., Rijnbrand, R.C., Amphlett, E., Clarke, B., Rowlands, D., Lemon, S.M., 1996. Structural requirements for initiation of translation by internal ribosome entry within genome-length hepatitis C virus RNA. Virology 222, 31–42.

Honda, M., Beard, M.R., Ping, L.H., Lemon, S.M., 1999a. A phylogenetically conserved stem-loop structure at the 5′ border of the internal ribosome entry site of hepatitis C virus is required for cap-independent viral translation. J. Virol. 73, 1165–1174.

Honda, M., Rijnbrand, R., Abell, G., Kim, D., Lemon, S.M., 1999b. Natural variation in translational activities of the 5′ nontranslated RNAs of hepatitis C virus genotypes 1a and 1b: evidence for a long-range RNA–RNA interaction outside of the internal ribosomal entry site. J. Virol. 73, 4941–4951.

Hwang, S.B., Lo, S.Y., Ou, J.H., Lai, M.M., 1995. Detection of cellular proteins and viral core protein interacting with the 5′ untranslated region of hepatitis C virus RNA. J. Biomed. Sci. 2, 227–236.

Isoyama, T., Kamoshita, N., Yasui, K., Iwai, A., Shiroki, K., Toyoda, H., Yamada, A., Takasaki, Y., Nomoto, A., 1999. Lower concentration of La protein required for internal ribosome entry on hepatitis C virus RNA than on poliovirus RNA. J. Gen. Virol. 80, 2319–2327.

Jubin, R., Vantuno, N.E., Kieft, J.S., Murray, M.G., Doudna, J.A., Lau, J.Y., Baroudy, B.M., 2000. Hepatitis C virus internal ribosome entry site (IRES) stem loop IIId contains a phylogenetically conserved GGG triplet essential for translation and IRES folding. J. Virol. 74, 10430–10437.

Kamoshita, N., Tsukiyama-Kohara, K., Kohara, M., Nomoto, A., 1997. Genetic analysis of internal ribosomal entry site on hepatitis C virus RNA: implication for involvement of the highly ordered structure and cell type-specific transacting factors. Virology 233, 9–18.

Kieft, J.S., Zhou, K., Jubin, R., Murray, M.G., Lau, J.Y., Doudna, J.A., 1999. The hepatitis C virus internal ribosome entry site adopts an ion-dependent tertiary fold. J. Mol. Biol. 292, 513–529.

Kieft, J.S., Zhou, K., Jubin, R., Doudna, J.A., 2001. Mechanism of ribosome recruitment by hepatitis C IRES RNA. RNA 7, 194–206.

Kim, Y.K., Lee, S.H., Kim, C.S., Seol, S.K., Jang, S.K., 2003. Long-range RNA–RNA interaction between the 5′ nontranslated region and the core-coding sequences of hepatitis C virus modulates the IRES-dependent translation. RNA 9, 599–606.

Kolupaeva, V.G., Pestova, T.V., Hellen, C.U., 2000. An enzymatic footprinting analysis of the interaction of 40S ribosomal subunits with the internal ribosomal entry site of hepatitis C virus. J. Virol. 74, 6242–6250.

Li, D., Takyar, S.T., Lott, W.B., Gowans, E.J., 2003. Amino acids 1–20 of the hepatitis C virus (HCV) core protein specifically inhibit HCV IRES-dependent translation in HepG2 cells, and inhibit both HCV IRES- and cap-dependent translation in HuH7 and CV-1 cells. J. Gen. Virol. 84, 815–825.

Lo, S.-Y., Selby, M.J., Ou, J.-H., 1996. Interaction between hepatitis C virus core protein and E1 envelope protein. J. Virol. 70, 5177–5182.

Lu, H.H., Wimmer, E., 1996. Poliovirus chimeras replicating under the translational control of genetic elements of hepatitis C virus reveal unusual

properties of the internal ribosomal entry site of hepatitis C virus. Proc. Natl. Acad. Sci. U.S.A. 93, 1412–1417.
Lukavsky, P.J., Otto, G.A., Lancaster, A.M., Samow, P., Puglisi, J.D., 2000. Structures of two RNA domains essential for hepatitis C virus internal ribosome entry site function. Nat. Struct. Biol. 7, 1105–1110.
Luo, G., Xin, S., Cai, Z., 2003. Role of the 5′-proximal stem-loop structure of the 5′ untranslated region in replication and translation of hepatitis C virus RNA. J. Virol. 77, 3312–3318.
Moriishi, K., Okabayashi, T., Nakai, K., Moriya, K., Koike, K., Murata, S., Chiba, T., Tanaka, K., Suzuki, R., Suzuki, T., Miyamura, T., Matsuura, Y., 2003. Proteasome activator PA28gamma-dependent nuclear retention and degradation of hepatitis C virus core protein. J. Virol. 77, 10237–10249.
Odreman-Macchioli, F.E., Tisminetzky, S.G., Zotti, M., Baralle, F.E., Buratti, E., 2000. Influence of correct secondary and tertiary RNA folding on the binding of cellular factors to the HCV IRES. Nucleic Acids Res. 28, 875–885.
Otto, G.A., Lukavsky, P.J., Lancaster, A.M., Samow, P., Puglisi, J.D., 2002. Ribosomal proteins mediate the hepatitis C virus IRES–HeLa 40S interaction. RNA 8, 913–923.
Pawlotsky, J.M., 2004. Pathophysiology of hepatitis C virus infection and related liver disease. Trends Microbiol. 12, 96–102.
Reynolds, J.E., Kaminski, A., Kettinen, H.J., Grace, K., Clarke, B.E., Carroll, A.R., Rowlands, D.J., Jackson, R.J., 1995. Unique features of internal initiation of hepatitis C virus RNA translation. EMBO J. 14, 6010–6020.
Rijnbrand, R.C.A., Lemon, S.M., 1999. Internal ribosomal entry site-mediated translation in hepatitis C virus replication. In: Hagedorn, C.H., Rice, C.M. (Eds.), The Hepatitis C Viruses. Springer-Verlag, Berlin, Germany, pp. 85–116.
Rijnbrand, R., Bredenbeek, P., van der Straaten, T., Whetter, L., Inchauspe, G., Lemon, S., Spaan, W., 1995. Almost the entire 5′ non-translated region of hepatitis C virus is required for cap-independent translation. FEBS Lett. 365, 115–119.
Santolini, E., Migliaccio, G., La Monica, N., 1994. Biosynthesis and biochemical properties of the hepatitis C virus core protein. J. Virol. 68, 3631–3641.
Shimoike, T., Mimori, S., Tani, H., Matsuura, Y., Miyamura, T., 1999. Interaction of hepatitis C virus core protein with viral sense RNA and suppression of its translation. J. Virol. 73, 9718–9725.
Sizova, D.V., Kolupaeva, V.G., Pestova, T.V., Shatsky, I.N., Hellen, C.U., 1998. Specific interaction of eukaryotic translation initiation factor 3 with the 5′ nontranslated regions of hepatitis C virus and classical swine fever virus RNAs. J. Virol. 72, 4775–4782.
Spahn, C.M., Kieft, J.S., Grassucci, R.A., Penczek, P.A., Zhou, K., Doudna, J.A., Frank, J., 2001. Hepatitis C virus IRES RNA-induced changes in the conformation of the 40s ribosomal subunit. Science 291, 1959–1962.
Spangberg, K., Schwartz, S., 1999. Poly(C)-binding protein interacts with the hepatitis C virus 5′ untranslated region. J. Gen. Virol. 80, 1371–1376.
Suzuki, R., Tamura, K., Li, J., Ishii, K., Matsuura, Y., Miyamura, T., Suzuki, T., 2001. Ubiquitin-mediated degradation of hepatitis C virus core protein is regulated by processing at its carboxyl terminus. Virology 280, 301–309.
Suzuki, R., Sakamoto, S., Tsutsumi, T., Rikimaru, A., Tanaka, K., Shimoike, T., Moriishi, K., Iwasaki, T., Mizumoto, K., Matsuura, Y., Miyamura, T., Suzuki, T., 2005. Molecular determinants for subcellular localization of hepatitis C virus core protein. J. Virol. 79, 1271–1281.
Takamizawa, A., Mori, C., Fuke, I., Manabe, S., Murakami, S., Fujita, J., Onishi, E., Andoh, T., Yoshida, I., Okayama, H., 1991. Structure and organization of the hepatitis C virus genome isolated from human carriers. J. Virol. 65, 1105–1113.
Tallet-Lopez, B., Aldaz-Carroll, L., Chabas, S., Dausse, E., Staedel, C., Toulme, J.J., 2003. Antisense oligonucleotides targeted to the domain IIId of the hepatitis C virus IRES compete with 40S ribosomal subunit binding and prevent in vitro translation. Nucleic Acids Res. 31, 734–742.
Tanaka, Y., Shimoike, T., Ishii, K., Suzuki, R., Suzuki, T., Ushijima, H., Matsuura, Y., Miyamura, T., 2000. Selective binding of hepatitis C virus core protein to synthetic oligonucleotides corresponding to the 5′ untranslated region of the viral genome. Virology 270, 229–236.
Tsukiyama-Kohara, K., Iizuka, N., Kohara, M., Nomoto, A., 1992. Internal ribosome entry site within hepatitis C virus RNA. J. Virol. 66, 1476–1483.
Wang, T.H., Rijnbrand, R.C., Lemon, S.M., 2000. Core protein-coding sequence, but not core protein, modulates the efficiency of cap-independent translation directed by the internal ribosome entry site of hepatitis C virus. J. Virol. 74, 11347–11358.
Zhang, J., Yamada, O., Yoshida, H., Iwai, T., Araki, H., 2002. Autogenous translational inhibition of core protein: implication for switch from translation to RNA replication in hepatitis C virus. Virology 293, 141–150.
Zhao, W.D., Wimmer, E., 2001. Genetic analysis of a poliovirus/hepatitis C virus chimera: new structure for domain II of the internal ribosomal entry site of hepatitis C virus. J. Virol. 75, 3719–3730.

JOURNAL OF CLINICAL MICROBIOLOGY, Sept. 2005, p. 4413–4417 Vol. 43, No. 9
0095-1137/05/$08.00+0 doi:10.1128/JCM.43.9.4413–4417.2005

Quantitative Detection of Hepatitis C Virus (HCV) RNA in Saliva and Gingival Crevicular Fluid of HCV-Infected Patients

Tetsuro Suzuki,[1]* Kazuhiko Omata,[1,2] Tazuko Satoh,[2] Takahiro Miyasaka,[2] Chiaki Arai,[3] Munehiro Maeda,[4] Tomonori Matsuno,[2] and Tatsuo Miyamura[1]

Department of Virology II, National Institute of Infectious Diseases,[1] Department of Oral and Maxillofacial Surgery[2] and Department of Endodontics and Operative Dentistry,[4] The Nippon Dental University School of Dentistry at Tokyo, and Section of Clinical Laboratory, The Nippon Dental University School of Dentistry at Tokyo Hospital,[3] Tokyo, Japan

Received 8 February 2005/Returned for modification 28 May 2005/Accepted 2 June 2005

The search for hepatitis C virus (HCV) in body fluids other than blood is important when assessing possible nonparenteral routes of viral transmission. However, the role of oral fluids in HCV transmission remains controversial. Here we quantitatively determined HCV RNA in saliva and gingival crevicular fluid (GCF) of anti-HCV-positive patients. Most patients (14 of 18; 78%) whose saliva specimens were negative had HCV RNA in their GCF. Most patients (20 of 26; 77%) had higher HCV RNA levels in their GCF than in their saliva. Although there was not a statistically significant correlation between the serum viral load and HCV level in saliva or GCF, patients with low serum HCV loads were less likely to have detectable HCV in their saliva. These findings have important implications for medical personnel and suggest that epidemiological studies designed to understand the significance of the oral route of transmission of HCV are warranted.

Hepatitis C virus (HCV) infection represents a major public health problem in the world today. The infection primarily causes liver disease; however, HCV infection has also been associated with extrahepatic abnormalities, including mixed cryoglobulinemia, malignant lymphoma, Sjögren's syndrome, and oral lichen planus (2, 12, 18, 19, 34, 39). Lymphotropism of HCV has been observed, and several laboratories have detected the virus in blood mononuclear cells (BMC) (16, 22, 26, 28, 35, 38). Common risk factors for HCV infection include blood transfusion from unscreened donors as well as injection drug use. Although sexual and vertical transmissions have also been reported, there remain a large number of HCV carriers in whom no route of infection has been identified.

Epidemiological surveys demonstrate that body fluids other than blood, including saliva, might be potential sources of HCV infection. Experimental inoculation of saliva obtained from chronic HCV carrier chimpanzees has been reported to transmit hepatitis to recipient animals (1). Several studies have demonstrated HCV RNA in the saliva of hepatitis C patients by reverse transcription (RT)-nested PCR. However, the detection rates of viral RNA within saliva have varied widely, and some groups have failed to demonstrate HCV RNA within saliva (6–11, 14, 17, 23, 25, 27, 29–33, 36–38). A potential source of HCV RNA within saliva includes gingival crevicular fluid (GCF), which might contain HCV-infected BMC in the setting of periodontal inflammation. To our knowledge, only one study has qualitatively identified HCV in GCF; HCV RNA was detected in 59% of GCF specimens from hepatitis C patients in the study (20). Since the efficiency of HCV transmission is likely related to its viral load, it is important to quantitate viral RNA levels within body fluids in order to properly evaluate possible nonparenteral routes of HCV infection.

Thus, we examined the presence of HCV RNA in the saliva and GCF of anti-HCV antibody-positive patients using real-time quantitative RT-PCR.

* Corresponding author. Mailing address: Department of Virology II, National Institute of Infectious Diseases, 2-14-15 Toyama, Shinjuku-ku, Tokyo, Japan 162-8640. Phone: (81) 3-5285-1111. Fax: (81) 3-5285-1161. E-mail: tesuzuki@nih.go.jp.

MATERIALS AND METHODS

Sample collection. Twenty-six dental patients attending the hospital of Nippon Dental University at Tokyo were studied. All of the patients were anti-HCV antibody seropositive on the basis of screening using a second-generation enzyme immunoassay (Abbott HCV PHA, Abbott Diagnostics, Abbott Park, IL). This study protocol was approved by the Ethics Committee of the hospital and was conducted according to *Ethic Guideline for the Studies on Human Genome and Gene Analysis*. Written informed consent was obtained from each patient participating in the study.

Blood samples were collected and centrifuged for 20 min at 5,000 rpm to separate the serum. Patients spit into a cup to obtain saliva samples. Whole saliva samples (approximately 2 ml) were then transferred into sterile containers. None of the samples were macroscopically observed to contain blood. GCF specimens were collected by first drying the gingival surface with sterile cotton, after which the area was isolated in order to prevent contamination with saliva. A paper strip (2 by 5 mm) was then subgingivally inserted for 30 s to collect specimens (approximately 50 μl). If there was visible contamination of the sample with blood, another sample without macroscopic blood contamination was taken from another site. The depth at gingival crevices was then measured by a periodontal probe, and the presence of bleeding on probing was examined. Serum, saliva, and GCF samples were collected simultaneously and were stored at −80°C before use.

RNA extraction. Total RNA was extracted from 100 μl of serum or saliva specimens and from paper strips with collected GCF using a QIAamp viral RNA kit (QIAGEN, Valencia, CA). In preliminary experiments using various amounts of serum, saliva, and GCF samples in the presence or absence of paper strips, we confirmed that (i) sample volumes of >40 μl yielded the same efficiencies of RNA extraction from each specimen and (ii) inclusion of a paper strip described above in the lysis buffer did not influence the efficiency of RNA extraction.

Quantitation of HCV RNA. To determine the quantity of HCV RNA, real-time RT-PCR involving single-tube reactions was performed using TaqMan EZ RT-PCR Core reagents (PE Applied Biosystems, Foster City, CA), as previously described (3). Briefly, the reaction mixture contained 1× TaqMan EZ buffer, 500 nM concentrations of each primer from the HCV 5′ noncoding region (5′-GAG TGT CGT GCA GCC TCC A-3′ and 5′-CAC TCG CAA GCA CCC TAT CA-3′), a 200 nM concentration of fluorogenic probe [5′-(6-carboxyfluorescein)

TABLE 1. Clinical and virological characteristics of 26 patients examined in this study[a]

Age	Gender	ALT level (IU/liter)	AST level (IU/liter)	HCV antibody titer (2^n)	Genotype	Oral disease(s)
68	F	30	48	>12	1b	
64	M	115	103	>12	1b	Periodontitis/BOP
71	F	14	23	12	2b	Periodontitis/BOP
71	M	124	71	12	1b	Periodontitis/BOP
71	M	47	55	12	1b	
63	M	14	19	11	1b	SCC
66	F	59	67	11	1b	OLP
61	F	61	35	11	1b	
73	F	48	40	10	2a	Periodontitis/BOP
70	F	18	25	10	1b	Periodontitis/BOP, OLP
72	F	15	20	8	1b	Periodontitis/BOP
61	M	7	12	8	ND	Periodontitis
66	F	19	30	8	1b	OLP
69	F	31	39	7	ND	SCC
73	M	16	24	6	ND	Periodontitis/BOP, SCC
72	F	20	22	6	ND	
67	M	12	18	4	ND	Periodontitis/BOP, SCC
70	F	5	17	4	ND	Periodontitis/BOP, SCC
69	M	13	20	4	1b	Periodontitis/BOP, SCC
60	M	22	23	4	1b	Periodontitis
71	F	15	30	4	ND	SCC
56	F	11	17	4	ND	Periodontitis/BOP, OLP
71	F	12	21	4	ND	Periodontitis/BOP
67	F	9	24	4	ND	
58	M	26	25	4	ND	
79	F	22	21	4	ND	

[a] Abbreviations: F, female; M, male; ND, not detected; OLP, oral lichen planus; BOP, bleeding on probing; SCC, squamous cell carcinoma.

CCC GCA AGA CTG CTA GCC GAG TAG TGT TGG (6-carboxytetramethylrhodamine)-3′], 200 μM concentrations of each deoxynucleoside triphosphate, 3 mM $Mn(OAc)_2$, 5 U of *Thermus thermophilus* DNA polymerase, 0.5 U of AmpErase uracil *N*-glycosylase, and template RNA. The primers and probe were designed on the basis of the conserved sequences among HCV genotypes. The RT step was started with a 1-min incubation at 50°C, followed by 50 min at 65°C. Thermal cycling conditions were as follows: a precycling period of 5 min at 95°Cfollowed by 50 cycles of denaturation at 94°C for 15 s and annealing at 55°C for 10 s and extension at 69°C for 1 min. All reactions and analyses of the amplification plots were performed on an Applied Biosystems PRISM 7700 sequence detector (PE Applied Biosystems). Standard curves of the assays were obtained by plotting 10-fold serial dilutions of known concentrations of a synthetic HCV genotype 1b transcript. HCV RNA copy numbers of the synthetic transcript were calculated from the quantity and its molecular weight. Using a standard curve, the Sequence Detector software calculated automatically the concentration of RNA copies in the experimental samples. We found that results obtained from our in-house real-time RT-PCR method were well correlated with those from the COBAS AMPLICOR HCV MONITOR Test, version 2.0 (Roche Diagnostics, Tokyo, Japan) (15), and that 1 HCV RNA copy/ml in our method corresponded to approximately 1 international unit/ml by the above-mentioned commercial assay (data not shown).

HCV genotyping. HCV genotype was determined by RT-PCR of the core region sequence with genotype-specific primers for determination of HCV genotypes 1a, 1b, 2a, 2b, 3a, 3b, 4, 5a, and 6a, as described previously (24).

PCR amplification of β-globin DNA. Total DNA was extracted from saliva samples using a QIAamp DNA Mini kit (QIAGEN) according to the manufacturer's instructions. To characterize the degree of cell contamination in saliva, isolated DNA was subsequently used as a template to amplify the human β-globin gene fragment of 268 bp with the following primers: 5′-GAA GAG CCA AGG ACA GGT AC-3′ and 5′-CAA CTT CAT CCA CGT TCA CC-3′ (21).

Statistical analysis. The Spearman rank test was used for evaluating the correlation between variables: anti-HCV antibody levels and viral loads in serum, saliva, and GCF.

RESULTS

The clinical and virological characteristics of 26 patients are presented in Table 1. The study group consisted of 10 males (38%) and 16 females (62%) with a mean age of 69 years (range, 56 to 79 years). Their mean liver enzyme values were as follows: 30 IU/liter for alanine aminotransferase (ALT) and 33 IU/liter for aspartic aminotransferase (AST). HCV RNA levels in the serum of 20 patients (77%) were determined by real-time RT-PCR assay, which showed a detection limit of 10^2 copies/ml and a linear range over 5 logs. Four of six serum samples whose HCV RNA levels were below the detection limit in this measurement were found to have detectable HCV RNA by the qualitative nested RT-PCR (4). We found no difference in efficiency and specificity of HCV cDNA amplification among genotypes 1b, 2a, and 2b in the real-time RT-PCR assay (data not shown).

Figure 1 summarizes viral loads in the serum, saliva, and GCF specimens of the patients. A mean serum HCV RNA level of 5.1×10^5 copies/ml was observed among samples with viral loads greater than 10^2 copies/ml. As expected, serum viral RNA levels were significantly correlated with anti-HCV antibody levels ($r = 0.80$, $P < 0.0001$) (Fig. 2A). In a number of cases (20 of 26; 77%), the viral load of the GCF was greater than that of the saliva. HCV RNA was detected in 31% of the saliva samples and 85% of the GCF specimens using real-time RT-PCR. Mean viral RNA levels were 1.9×10^4 (saliva) and 3.1×10^4 (GCF) copies/ml in these samples. It should be noted that most (seven out of eight) of the saliva samples contained 1.4×10^2 to 8.2×10^3 copies/ml of HCV RNA, with a mean value of 2.0×10^3 copies/ml among these seven samples (Fig. 1).

Among the 18 patients with HCV RNA-negative saliva, 10^2 to 10^3 copies/ml of viral RNA were detected in the GCF of 3 patients, 10^3 to 10^4 copies/ml of viral RNA were detected in the GCF of 2 patients, and $>10^4$ copies/ml were detected in

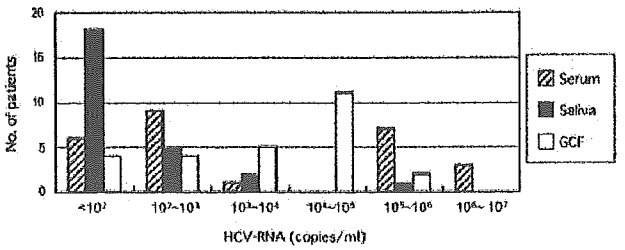

FIG. 1. HCV viral load in the serum, saliva, and GCF of anti-HCV-positive patients. Numbers of patients within each range of the viral load are indicated.

the GCF of 9 patients. No significant association was observed between viral RNA levels in the serum and viral RNA levels in the saliva (Fig. 2B) or GCF (Fig. 2C). However, relatively high serum viral loads ($>10^5$ copies/ml) were observed in five out of eight patients with HCV RNA-positive saliva, while serum viral loads were 1.5×10^3 copies/ml or less in most of the patients whose saliva specimens were negative (13 out of 18). Four patients with HCV RNA-positive saliva and/or GCF had no detectable serum HCV RNA by real-time RT-PCR (Fig. 2B and C); however, viral RNA was detectable in their sera by qualitative nested RT-PCR. Although no visible contamination of the saliva and GCF with blood was observed, there may be a small amount of cells or lysed cells in the fluids. To determine the degree of cell content in samples, total DNA was extracted from three saliva specimens, which contained $>10^3$ copies/ml of HCV RNA (Fig. 2B), and tested for the presence of cellular DNA by amplifying a human β-globin gene. A certain amount of cellular DNA was detectable in the saliva specimens (data not shown), suggesting some salivary HCV RNA may be derived from HCV-infected cells, such as BMC and mucosal epithelial cells, as discussed below. Various amounts of HCV-infected cells in the saliva and GCF may, in part, account for differences in the viral loads.

HCV RNA was detectable in most GCF and/or saliva specimens obtained from patients with clinical evidence of oral diseases: HCV RNA was detected in all 14 (100%) patients with periodontitis, 6 of 7 (85%) patients with squamous cell carcinoma, and 3 of 4 (75%) patients with lichen planus. Three out of four patients with HCV RNA-negative GCF, however, also had some oral epithelial lesions. On the other hand, among seven patients without oral diseases, HCV RNA was detected in the GCF and saliva of six and three patients, respectively. There was a trend toward increased viral loads in the oral fluids, especially GCF, among patients with bleeding on probing compared to those without the bleeding. The viral RNA levels in the GCF and saliva had no correlation with age, gender, or serum levels of ALT or AST. It also seems that their viral RNA levels were not correlated with HCV genotype, although the viral genotypes in 12 of 26 patients were not determined.

DISCUSSION

Identification of HCV in body fluids other than blood is important in order to evaluate possible nonparenteral routes of transmission. The role of oral fluids in HCV transmission remains controversial. Although the presence of HCV RNA in saliva has been reported by several research groups (6–11, 14, 17, 23, 25, 27, 29–33, 36–38), only one study has attempted to quantify HCV RNA in saliva, in which patients coinfected with HCV and human immunodeficiency virus were examined using a branched DNA assay (27). Moreover, limited information exists regarding the prevalence of HCV in the GCF of patients with hepatitis C, apart from one study in which a qualitative RT-PCR method was used to detect HCV in 59% of GCF and 35% of saliva specimens from patients with HCV viremia (20).

To the best of our knowledge, this study is the first to quantitate HCV loads within the saliva and GCF of anti-HCV antibody-positive patients using real-time RT-PCR. To search for a possible oral route of HCV transmission, whole saliva and GCF containing cell fractions were used to determine the viral

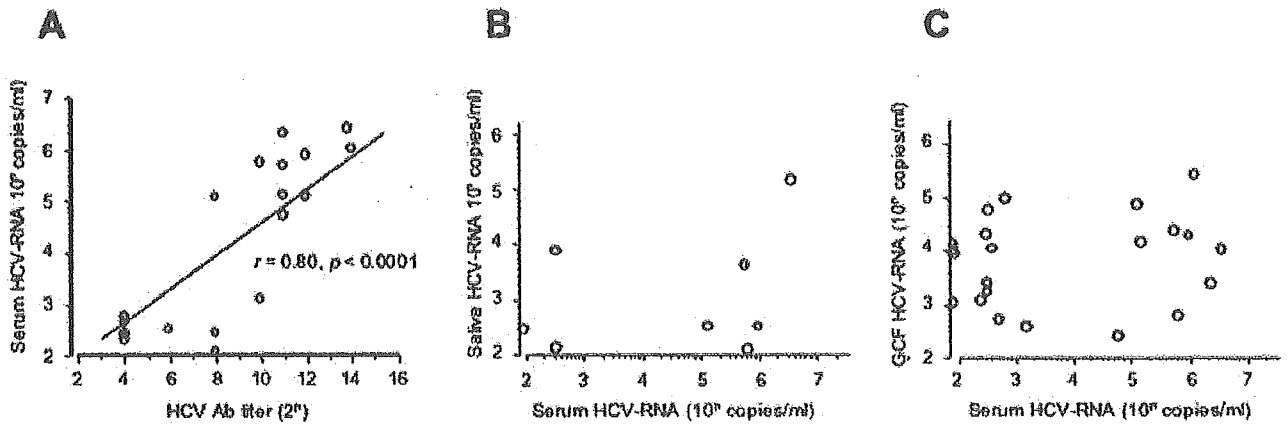

FIG. 2. (A) Correlation between anti-HCV antibody levels and HCV RNA levels in serum. The Spearman rank test was used for testing the correlation between variables. There is a significant positive correlation ($r = 0.80$, $P < 0.0001$) between the serum levels of HCV antibody detected by the passive hemagglutination assay and those of HCV RNA determined by real-time RT-PCR. (B) Correlation between viral loads in the serum and those in saliva specimens. Results for patients whose HCV RNA levels in saliva were $\geq 10^2$ copies/ml are plotted. No significant correlation was observed. (C) Correlation between viral loads in serum and those in GCF specimens. Results for patients whose HCV RNA levels in the GCF were $\geq 10^2$ copies/ml are plotted. No significant correlation was observed.

loads in this study. Although any saliva and GCF samples tested were not macroscopically observed to contain blood, we cannot rule out the possible effect of a small amount of bleeding as a source of HCV RNA. Here we observed HCV more commonly in the GCF than the saliva of HCV-seropositive patients. We further found viral loads of 10^2 to 10^4 copies/ml and 10^3 to 10^5 copies/ml in saliva and GCF, respectively. This result may be partially due to the presence of PCR inhibitors in saliva. An internal control to measure the possible effect of PCR inhibitors was not included in our real-time RT-PCR. Although the mean viral load within the GCF was approximately 10-fold lower than that in the serum, GCF samples from 12 of 26 patients (46%) had viral titers similar to or greater than those observed in the sera. No significant correlation was observed between the serum viremia levels and viral levels in the saliva or GCF. However, there was a trend that patients with HCV RNA-positive saliva showed higher viral loads in sera than patients with HCV RNA-negative saliva. These findings suggest that GCF might be one of the sources of HCV RNA within the saliva.

Although HCV is a hepatotropic virus, convincing evidence of HCV lymphotropism has been demonstrated in tissue culture (13). HCV has been widely detected in BMC in patients with chronic HCV infection, and differences in quasispecies identification within serum and BMC suggest that viral replication occurs within BMC (16, 22, 26, 28, 35, 38). HCV-infected BMC might allow HCV to infiltrate the GCF and saliva, since BMC migrate from dentogingival vessels into gingival crevices. There also might be transudation of HCV-containing serum into the mouth. Generally, periodontal inflammation increases the excretion of BMC-rich GCF. There is also a possibility that HCV exists within mucosal epithelial cells. HCV has been identified in the mucosal tissue, as well as salivary glands, of anti-HCV-positive patients with oral lichen planus using various techniques, including in situ hybridization, strand-specific RT-PCR, and immunohistochemistry (5, 32). Thus, it is likely that several possible sources discussed above are involved in HCV penetration into the saliva and GCF. Whatever the sources or mechanisms are, the findings obtained provide important implications for medical personnel regarding HCV transmission in health care settings as well as for HCV epidemiology, as the origin of the viral infection remains unclear in up to 40% of cases.

In this study, although the numbers of specimens were limited, we quantitatively determined HCV RNA in oral fluids from dental patients, including some patients with oral diseases, and demonstrated frequent detection of HCV in the saliva and GCF. Further large-scale epidemiological studies employing real-time RT-PCR assays are required to clarify the clinical significance of HCV in the saliva and GCF, including the potential for viral transmission through exposure to these fluids.

ACKNOWLEDGMENTS

We thank Yasushi Inoue and Ryosuke Suzuki for technical advice and helpful discussion on data analysis. We also thank Makiko Yahata for technical assistance and Tomoko Mizoguchi for manuscript preparation.

This work was partly supported by grants-in-aid from the Ministry of Health, Labor, and Welfare of Japan to T.S. and T.S.

REFERENCES

1. **Abe, K., and G. Inchauspe.** 1991. Transmission of hepatitis C by saliva. Lancet **337**:248.
2. **Aceti, A., G. Taliani, M. Sorice, and M. A. Amendolea.** 1992. HCV and Sjogren's syndrome. Lancet **339**:1425–1426.
3. **Aizaki, H., K. J. Lee, V. M. Sung, H. Ishiko, and M. M. Lai.** 2004. Characterization of the hepatitis C virus RNA replication complex associated with lipid rafts. Virology **324**:450–461.
4. **Aizaki, H., A. Saito, I. Kusakawa, Y. Ashiwara, S. Nagamori, G. Toda, T. Suzuki, K. Ishii, Y. Matsuura, and T. Miyamura.** 1996. Mother-to-child transmission of a hepatitis C virus variant with an insertional mutation in its hypervariable region. J. Hepatol. **25**:608–613.
5. **Arrieta, J. J., E. Rodriguez-Inigo, N. Ortiz-Movilla, J. Bartolome, M. Pardo, F. Manzarbeitia, H. Oliva, D. M. Macias, and V. Carreno.** 2001. In situ detection of hepatitis C virus RNA in salivary glands. Am. J. Pathol. **158**: 259–264.
6. **Chen, M., Z. B. Yun, M. Sallberg, R. Schvarcz, I. Bergquist, H. B. Berglund, and A. Sonnerborg.** 1995. Detection of hepatitis C virus RNA in the cell fraction of saliva before and after oral surgery. J. Med. Virol. **45**:223–226.
7. **Couzigou, P., L. Richard, F. Dumas, L. Schouler, and H. Fleury.** 1993. Detection of HCV-RNA in saliva of patients with chronic hepatitis C. Gut **34**:S59–S60.
8. **Fabris, P., D. Infantolino, M. R. Biasin, G. Marchelle, E. Venza, V. Terribile Wiel Marin, P. Benedetti, G. Tositti, V. Manfrin, and F. de Lalla.** 1999. High prevalence of HCV-RNA in the saliva cell fraction of patients with chronic hepatitis C but no evidence of HCV transmission among sexual partners. Infection **27**:86–91.
9. **Fried, M. W., M. Shindo, T. L. Fong, P. C. Fox, J. H. Hoofnagle, and A. M. Di Bisceglie.** 1992. Absence of hepatitis C viral RNA from saliva and semen of patients with chronic hepatitis C. Gastroenterology **102**:1306–1308.
10. **Hermida, M., M. C. Ferreiro, S. Barral, R. Laredo, A. Castro, and P. Diz Dios.** 2002. Detection of HCV RNA in saliva of patients with hepatitis C virus infection by using a highly sensitive test. J. Virol. Methods **101**:29–35.
11. **Hsu, H. H., T. L. Wright, D. Luba, M. Martin, S. M. Feinstone, G. Garcia, and H. B. Greenberg.** 1991. Failure to detect hepatitis C virus genome in human secretions with the polymerase chain reaction. Hepatology **14**:763–767.
12. **Imhof, M., H. Popal, J. H. Lee, S. Zeuzem, and R. Milbradt.** 1997. Prevalence of hepatitis C virus antibodies and evaluation of hepatitis C virus genotypes in patients with lichen planus. Dermatology **195**:1–5.
13. **Kato, N.** 1999. Systems to culture hepatitis C virus, p. 261–278. *In* C. H. Hagedorn and C. M. Rice (ed.), The hepatitis C virus. Springer-Verlag, Berlin, Germany.
14. **Komiyama, K., F. Kawamura, Y. Arakawa, H. Mastuo, N. Hayashi, T. Shikata, and I. Moro.** 1995. Detection of hepatitis C virus (HCV)-RNA in saliva and gastric juice. Adv. Exp. Med. Biol. **371B**:995–997.
15. **Lee, S. C., A. Antony, N. Lee, J. Leibow, J. Q. Yang, S. Soviero, K. Gutekunst, and M. Rosenstraus.** 2000. Improved version 2.0 qualitative and quantitative AMPLICOR reverse transcription-PCR tests for hepatitis C virus RNA: calibration to international units, enhanced genotype reactivity, and performance characteristics. J. Clin. Microbiol. **38**:4171–4179.
16. **Lerat, H., S. Rumin, F. Habersetzer, F. Berby, M. A. Trabaud, C. Trepo, and G. Inchauspe.** 1998. In vivo tropism of hepatitis C virus genomic sequences in hematopoietic cells: influence of viral load, viral genotype, and cell phenotype. Blood **91**:3841–3849.
17. **Liou, T. C., T. T. Chang, K. C. Young, X. Z. Lin, C. Y. Lin, and H. L. Wu.** 1992. Detection of HCV RNA in saliva, urine, seminal fluid, and ascites. J. Med. Virol. **37**:197–202.
18. **Lunel, F., and L. Musset.** 1996. Hepatitis C virus infection and cryoglobulinemia. Viral Hepatitis Rev. **2**:111–124.
19. **Mariette, X., M. Zerbib, A. Jaccard, C. Schenmetzler, F. Danon, and J. P. Clauvel.** 1993. Hepatitis C virus and Sjogren's syndrome. Arthritis Rheum. **36**:280–281.
20. **Maticic, M., M. Poljak, B. Kramar, K. Seme, V. Brinovec, J. Meglic-Volkar, B. Zakotnik, and U. Skaleric.** 2001. Detection of hepatitis C virus RNA from gingival crevicular fluid and its relation to virus presence in saliva. J. Periodontol. **72**:11–16.
21. **McElhinney, L. M., R. J. Cooper, and D. J. Morris.** 1995. Multiplex polymerase chain reaction for human herpesvirus-6, human cytomegalovirus, and human beta-globin DNA. J. Virol. Methods **53**:223–233.
22. **Muller, H. M., E. Pfaff, T. Goeser, B. Kallinowski, C. Solbach, and L. Theilmann.** 1993. Peripheral blood leukocytes serve as a possible extrahepatic site for hepatitis C virus replication. J. Gen. Virol. **74**:669–676.
23. **Numata, N., H. Ohori, Y. Hayakawa, Y. Saitoh, A. Tsunoda, and A. Kanno.** 1993. Demonstration of hepatitis C virus genome in saliva and urine of patients with type C hepatitis: usefulness of the single round polymerase chain reaction method for detection of the HCV genome. J. Med. Virol. **41**:120–128.
24. **Ohno, O., M. Mizokami, R. R. Wu, M. G. Saleh, K. Ohba, E. Orito, M. Mukaide, R. Williams, and J. Y. Lau.** 1997. New hepatitis C virus (HCV) genotyping system that allows for identification of HCV genotypes 1a, 1b, 2a, 2b, 3a, 3b, 4, 5a, and 6a. J. Clin. Microbiol. **35**:201–207.

25. **Puchhammer-Stockl, E., W. Mor, M. Kundi, F. X. Heinz, H. Hofmann, and C. Kunz.** 1994. Prevalence of hepatitis-C virus RNA in serum and throat washings of children with chronic hepatitis. J. Med. Virol. **43**:143–147.
26. **Qian, C., J. Camps, M. D. Maluenda, M. P. Civeira, and J. Prieto.** 1992. Replication of hepatitis C virus in peripheral blood mononuclear cells. Effect of alpha-interferon therapy. J. Hepatol. **16**:380–383.
27. **Rey, D., S. Fritsch, C. Schmitt, P. Meyer, J. M. Lang, and F. Stoll-Keller.** 2001. Quantitation of hepatitis C virus RNA in saliva and serum of patients coinfected with HCV and human immunodeficiency virus. J. Med. Virol. **63**:117–119.
28. **Roque Afonso, A. M., J. Jiang, F. Penin, C. Tareau, D. Samuel, M. A. Petit, H. Bismuth, E. Dussaix, and C. Feray.** 1999. Nonrandom distribution of hepatitis C virus quasispecies in plasma and peripheral blood mononuclear cell subsets. J. Virol. **73**:9213–9221.
29. **Roy, K. M., J. Bagg, G. L. Bird, E. Spence, E. A. Follett, P. R. Mills, and J. Y. Lau.** 1995. Serological and salivary markers compared with biochemical markers for monitoring interferon treatment for hepatitis C virus infection. J. Med. Virol. **47**:429–434.
30. **Roy, K. M., J. Bagg, B. McCarron, T. Good, S. Cameron, and A. Pithie.** 1998. Predominance of HCV type 2a in saliva from intravenous drug users. J. Med. Virol. **54**:271–275.
31. **Sugimura, H., H. Yamamoto, H. Watabiki, H. Ogawa, H. Harada, I. Saitoh, T. Miyamura, M. Inoue, K. Tajima, and I. Kino.** 1995. Correlation of detectability of hepatitis C virus genome in saliva of elderly Japanese symptomatic HCV carriers with their hepatic function. Infection **23**:258–262.
32. **Takamatsu, K., I. Okayasu, Y. Koyanagi, and N. Yamamoto.** 1992. Hepatitis C virus propagates in salivary glands. J. Infect. Dis. **165**:973–974.
33. **Taliani, G., D. Celestino, M. C. Badolato, A. Pennica, A. Bozza, G. Poliandri, V. Riccieri, G. Benfari, A. Sebastiani, C. De Bac, G. Quaranta, and A. Aceti.** 1997. Hepatitis C virus infection of salivary gland epithelial cells. Lack of evidence. J. Hepatol. **26**:1200–1206.
34. **Vincent, A.** 2000. Mixed cryoglobulinemia and other extrahepatic manifestations of hepatitis C virus infection, p. 295–313. *In* T. J. Liang and J. H. Hoofnagle (ed.), Hepatitis C. Biomedical research reports. Academic Press, San Diego, Calif.
35. **Wang, J. T., J. C. Shen, J. T. Lin, T. H. Wang, and D. S. Chen.** 1992. Detection of replicative form of hepatitis C virus RNA in peripheral blood mononuclear cells. J. Infect. Dis. **166**:1167–1169.
36. **Wang, J. T., T. H. Wang, J. T. Lin, J. C. Shen, S. M. Lin, and D. S. Chen.** 1991. Hepatitis C virus RNA in saliva of patients with post-transfusion hepatitis C infection. Lancet **337**:48.
37. **Wang, J. T., T. H. Wang, J. C. Shen, J. T. Lin, and D. S. Chen.** 1992. Hepatitis C virus RNA in saliva of patients with posttransfusion hepatitis and low efficiency of transmission among spouses. J. Med. Virol. **36**:28–31.
38. **Young, K. C., T. T. Chang, T. C. Lion, and H. L. Wu.** 1993. Detection of hepatitis C virus RNA in peripheral blood mononuclear cells and in saliva. J. Med. Virol. **41**:55–60.
39. **Zoulim, F., M. Chevallier, M. Maynard, and C. Trepo.** 2003. Clinical consequences of hepatitis C virus infection. Rev. Med. Virol. **13**:57–68.

JOURNAL OF VIROLOGY, May 2005, p. 5337–5345 Vol. 79, No. 9
0022-538X/05/$08.00+0 doi:10.1128/JVI.79.9.5337–5345.2005

Structure and Assembly of a $T=1$ Virus-Like Particle in BK Polyomavirus

Josefina Nilsson,[1] Naoyuki Miyazaki,[1] Li Xing,[1] Bomu Wu,[1] Lena Hammar,[1] Tian Cheng Li,[2] Naokazu Takeda,[2] Tatsuo Miyamura,[2] and R. Holland Cheng[1,3]*

Department of Biosciences at Novum, Karolinska Institute, 14157 Huddinge, Sweden[1]; Department of Virology II, National Institute of Infectious Diseases, Tokyo 162-8640, Japan[2]; and Molecular and Cellular Biology, University of California, Davis, California 95616[3]

Received 27 July 2004/Accepted 7 December 2004

In polyomaviruses the pentameric capsomers are interlinked by the long C-terminal arm of the structural protein VP1. The $T=7$ icosahedral structure of these viruses is possible due to an intriguing adaptability of this linker arm to the different local environments in the capsid. To explore the assembly process, we have compared the structure of two virus-like particles (VLPs) formed, as we found, in a calcium-dependent manner by the VP1 protein of human polyomavirus BK. The structures were determined using electron cryomicroscopy (cryo-EM), and the three-dimensional reconstructions were interpreted by atomic modeling. In the small VP1 particle, 26.4 nm in diameter, the pentameric capsomers form an icosahedral $T=1$ surface lattice with meeting densities at the threefold axes that interlinked three capsomers. In the larger particle, 50.6 nm in diameter, the capsomers form a $T=7$ icosahedral shell with three unique contacts. A folding model of the BKV VP1 protein was obtained by alignment with the VP1 protein of simian virus 40 (SV40). The model fitted well into the cryo-EM density of the $T=7$ particle. However, residues 297 to 362 of the C-terminal arm had to be remodeled to accommodate the higher curvature of the $T=1$ particle. The loops, before and after the C-terminal short helix, were shown to provide the hinges that allowed curvature variation in the particle shell. The meeting densities seen at the threefold axes in the $T=1$ particle were consistent with the triple-helix interlinking contact at the local threefold axes in the $T=7$ structure.

The BK virus (BKV) is a human virus belonging to the *Polyomaviridae* family. It is a nonenveloped virus (~50.0 nm in diameter) with a circular double-stranded DNA genome (~5 kb). The capsid has icosahedral symmetry and is built of 72 capsomers that are all pentamers of the protein VP1 arranged in a $T=7$ icosahedral lattice (21). All known polyomaviruses have three structural proteins (VP1, VP2, and VP3), of which VP1 is the major capsid protein. Overall amino acid sequence homology between BKV and the other human polyomavirus, JCV, is 75%, and that with the simian polyomavirus (SV40) is 69% (9). In the VP1 protein the sequence similarity rises to 77% and 74% for the JCV and SV40, respectively (35). Due to the high similarity, the solved atomic structure of VP1 of SV40 provides us a template to create a model of the BKV VP1 protein folding.

The structures of the SV40 and murine polyomavirus have been determined and show similar features to that seen in the BKV (1, 12). The VP1 pentamer of SV40 and murine polyomavirus is built as a ring of five β-barrel-shaped VP1 monomers, tightly linked by interacting loops between the framework of β-strands (22, 33, 34, 40). The C-terminal subdomain of each VP1 monomer "invades" a neighboring pentamer, thereby tying the pentamers together in the virion shell. There are six unique monomers building up the capsid (monomer α, α′, and α″ at the local threefold; β, β′ around the icosahedral threefold, and γ at the twofold) (34). The major structural differences between the six unique monomers are found in their C termini and are essential for the formation of the icosahedral capsid. The most flexible region seemed to be the outermost C terminus of the peptide chain (amino acids 355 to 364). The structure of this region has not been defined in three of the six unique monomers (α, α″, and β).

Under certain conditions the polyomavirus capsid disassembles into pentamers, which can be reassembled. The reassembled particle may have different configurations and sizes depending on the buffer conditions. This was shown for recombinant SV40 VLPs (17) and recombinant murine polyoma VLPs (28, 29). In the latter case, Salunke et al. (29) demonstrated that three differently sized VLPs appeared, depending on the buffer conditions. They concluded through computational modeling that two of the reassembled murine polyomavirus particles had icosahedral symmetry and were composed of 12 and 72 pentamers, in a $T=1$ and $T=7$, respectively, surface lattice. The third particle was composed of 24 pentamers with an octahedral symmetry.

Many studies have demonstrated that calcium ions play an important role in viral assembly (3, 5, 6, 13, 14, 17, 20, 25, 26, 28). Besides the calcium-binding site, disulfide bonds have also been found to be involved in maintaining capsid stability of the polyomavirus (5, 6, 11, 14, 15, 19, 30, 36). Interpentameric disulfide linkages have been revealed by X-ray crystallography in the capsid structure of SV40 and murine polyomavirus (22, 33, 34).

* Corresponding author. Mailing address: Department of Molecular and Cellular Biology, University of California, Davis, CA 95616. Phone: (530) 752-3611. Fax: (530) 752-3085. E-mail: rhch@ucdavis.edu.

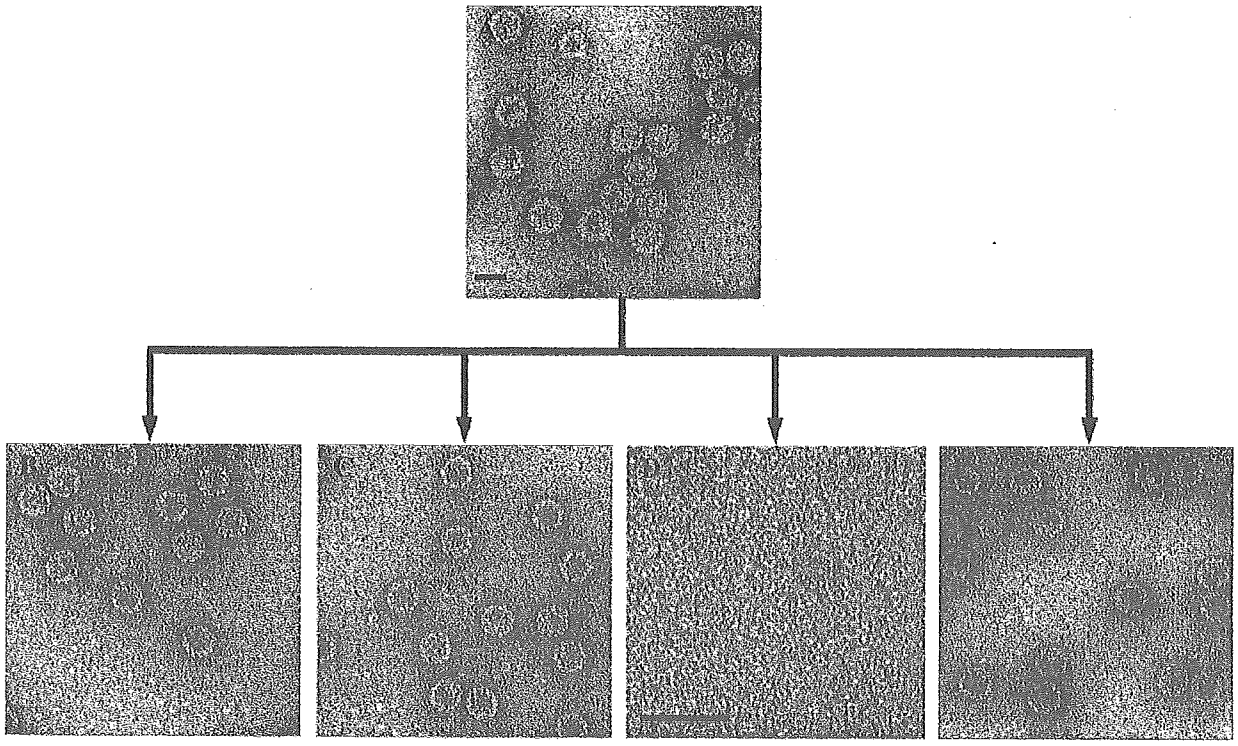

FIG. 1. Factors guiding disassembly of BKV VLPs. (A) Electron micrograph (negative stained) of recombinant BKV VLPs (0.5 mg/ml). To find dissociation conditions, the BKV VLPs (A) were equilibrated by dialysis against different concentrations of EDTA (10 to 100 mM), 2-ME (10 to 100 mM), and NaCl (0.15 to 1 M). All experiments were done overnight at room temperature, and the resulting appearance of the samples are shown in the electron micrographs B to E (negative stain). (B) Result from dialysis against 20 mM EDTA. (C) Result from dialysis against 30 mM 2-ME. (D) Result from dialysis against 20 mM EDTA and 30 mM 2-ME. (E) Result from dialysis against 20 mM EDTA, 30 mM 2-ME, and 0.6 M NaCl. Bars, 50 nm.

The gene of the major structural protein of the BKV VP1 was recently expressed in Tn5 cells using a recombinant baculovirus vector (21). The BKV VP1 self-assembled into VLPs in the nucleus, and the particles were then efficiently released into the culture medium. These VLPs possessed similar antigenicity as native BKV particles and were indistinguishable as negative-stained specimens in electron microscopy. The structure was determined to 2.0 nm resolution, using electron cryomicroscopy (cryo-EM) and three-dimensional reconstruction, and showed similar features to both SV40 and murine polyomavirus.

Here, we report for the first time the three-dimensional structure of a smaller BKV VLP determined by cryo-EM, image reconstruction, and docking of the VP1 model. We compare the structure of the two different BKV VLPs and explore the in vitro disassembly/reassembly process of them.

MATERIALS AND METHODS

Expression and purification of the BKV capsid protein VP1. For the large-scale expression of the BKV capsid protein VP1 (21, 37), an insect cell line from *Trichoplusia ni*, BTL-Tn 5B1-4 (Tn5) (Invitrogen, San Diego, CA) was used. Tn5 cells were infected with recombinant baculoviruses at a multiplicity of infection (MOI) of 10 and were incubated in EX-CELL 405 medium (JRH Biosciences, Lenexa, KS) for 7 days at 26.5°C. Intact cells, cell debris, and progeny baculoviruses were removed by centrifugation at 10,000 × *g* for 90 min. The supernatant was then spun at 25,000 rpm for 2 h in a Beckman SW28 rotor. The resulting pellet was resuspended in 4.5 ml of EX-CELL 405 at 4°C overnight. After mixing

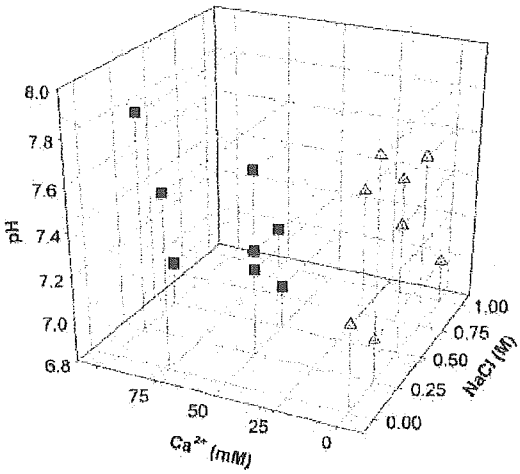

FIG. 2. Effect of buffer composition on the shape of reassembled particles. When the VLPs had been dissociated, the sample (now containing free pentamers) was dialyzed again against buffers with different concentrations of a monovalent salt, NaCl (0.0 to 1.0 M), pH (7.0 to 7.8), and a divalent ion, Ca^{2+} (0.0 to 100.0 mM). Square: buffer conditions when less then 30% of the reassembled particles had a $T=1$ symmetry. Triangle: buffer conditions when more then 80% of the reassembled particles had a $T=1$ symmetry. All experiments were done at room temperature and overnight.

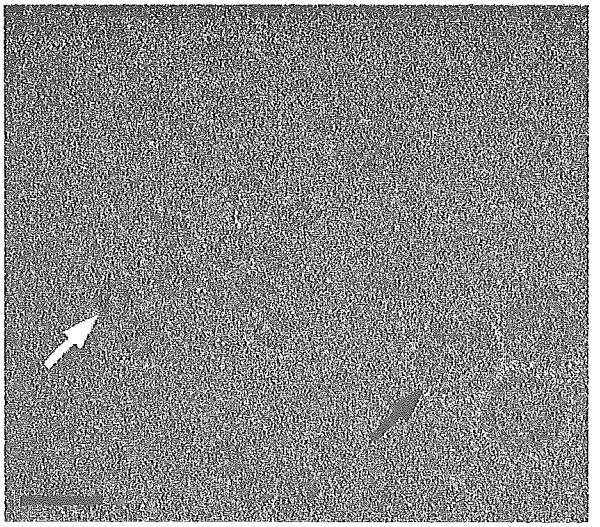

FIG. 3. Cryo-electron micrograph of BKV VLPs that were reassembled after overnight equilibration against 5 mM Ca^{2+}, 150 mM NaCl, and 10 mM Tris-HCl, pH 7.4. Two populations of BKV VLPs that differed in size can be seen (white arrow, small VLP; black arrow, large native-size VLP). Bar, 50 nm.

with 2.1 g of CsCl, the sample was centrifuged at 35,000 rpm for 24 h at 4°C in a Beckman SW50.1 rotor. Four bands were harvested by puncturing the tubes with a 22-gauge needle. To remove the CsCl, each band was diluted 10× and centrifuged for 2 h in a Beckman TLA55 rotor at 50,000 rpm; the pellet was then resuspended in 150 mM NaCl, 10 mM TRIS-HCl, pH 7.4.

Dialysis experiments. To screen for factors effecting dissociation and reassembly of the BKV VLPs, a homemade dialysis equipment that allowed dialyses of small amounts of sample (20 to 40 μl) was used. BKV VLPs (35 μl, 0.5 mg/ml) were first dialyzed against different concentrations of EDTA (10 to 100 mM),

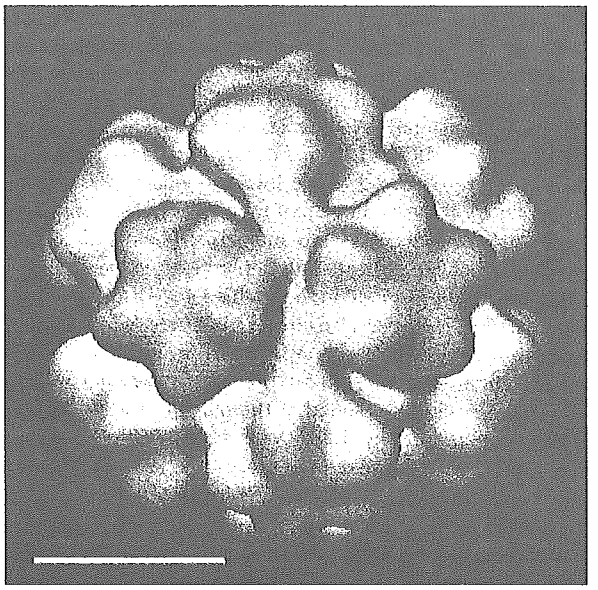

FIG. 4. Cryo-EM three-dimensional reconstruction of the small BKV VLP from Fig. 3. The particle is viewed along the twofold axis. It has icosahedral symmetry, and the VP1 protein establishes an arrangement according to a $T=1$ lattice with protruding capsomer at each fivefold. Bar, 10 nm.

2-mercaptoethanol (2-ME) (10 to 100 mM), and NaCl (0.15 to 1 M) in an attempt to dissociate the VLPs. When the VLPs had been dissociated, the sample (now containing free pentamers) was again dialyzed against buffers with different concentrations of a monovalent salt, NaCl (0.0 to 1.0 M), pH (7.0 to 7.8), and a divalent ion, Ca^{2+} (0.0 to 100.0 mM), to make the pentamers reassemble into VLPs. All experiments were done in room temperature and overnight. The selection of conditions for the second dialysis, like combinations of different pH, calcium, and NaCl concentrations, was done with the aid of the software DESIGN (32).

To determine the proportion of small (26.4 nm in diameter) and large VLPs (50.6 nm in diameter) in the different reassembly experiments, samples were applied to carbon-coated grids, negatively stained, and checked by EM. Thirty fields were randomly chosen from each grid and micrograph taken. In each the numbers of small and large VLPs were counted.

Negative contrasting electron microscopy. For EM, a sample of ~3 μl was applied to the charged grid and allowed to settle for 20 seconds. The solution was removed by blotting with a filter paper and the sample washed once with 3 μl of water for 15 seconds before stained with a 2% uranyl acetate solution. After 15 seconds the uranyl acetate solution was blotted off with a filter paper. The samples were observed by a Philips CM120 electron microscope.

Cryo-electron microscopy and three-dimensional image analysis. Frozen-hydrated specimens were prepared by applying 3.0-μl droplets of an aqueous mixture of reassembled BKV VLPs (1.0 to 1.5 mg/ml) on 300-mesh copper grids coated with holey carbon film. The images of the frozen VLPs were recorded with a Philips CM120 (Philips Electronics Instruments) by defined low-dose condition. The micrographs were taken with Kodak SO163 films (Eastman Kodak Co., New York, NY) at 45,000 nominal magnifications and 120 kV operating voltage. Each area of specimen was recorded twice as focal pairs with defocus value of 1.0 and 3.0 μm, respectively (38). Micrographs with sufficiently separated and well-distributed particles, exhibiting minimal astigmatism, were digitized at 14-μm intervals (0.311-nm sampling at the specimen) with a Zeiss microdensitometer. Individual particle images were extracted and analyzed with icosahedral symmetry processing procedures to reconstruct the three-dimensional structure (39). Computations were performed with interactive FORTRAN programs on Alphastations (Digital Equipment Co., MA).

The initial phase origins of selected particle images were obtained by using a cross-correlation method, where the particle orientations were determined through modified self-common-lines and polar Fourier transform procedures (2, 10). This was followed by interparticle orientation refinement with increasing numbers of unique images by cross-common-lines procedures. To improve the sensitivity and reliability of the orientation refinement procedures with the BKV VLPs images, the data were Fourier-filtered to remove both low- and high-frequency noise beyond the processing regions. Refinement of origins and orientations was repeated in cycles at progressively higher spatial frequencies until no further improvement was found in the common-lines phase residues. Besides the procedures described above, back-projection images of the preliminary reconstruction were used as references to accurately refine the phase origins and orientations of the corresponding images. The resolution was progressively improved and the final three-dimensional reconstruction was computed to a resolution of 2.4 nm, which was within the limit imposed by the first zero of the contrast transfer function of the electron microscope.

Fitting of BKV VP1 model into the EM density map. The atomic model of BK VP1 protein was constructed from SV40 VP1 using the SWISS-MODEL Protein Modeling Server (31) and the software modeler. Following that, the fitting of the pentameric structures to the cryo-EM map of the $T=1$ particle was performed manually using O (16) based on one of the pentamers from the BKV $T=7$ capsid. We used the VP1 pentameric model of BKV at the pentavalent position in the $T=7$ particles to build the atomic model of the $T=1$ particles. For the initial fitting, only the core of the VP1 was used, which consists of residues 16 to 296. This was based on the fact that the conformation of this pentameric structure was almost the same, with root mean-square deviations (rmsd) of less than 0.1 nm, as that in a $T=7$ particle.

Further, in the final stage of fitting, the position of the pentamer was optimized by the reciprocal-space rigid-body refinement between the cryo-EM map and the models. The amino acid residues 297 to 330 connecting the neighboring pentamers were omitted in this procedure. The cryo-EM map was moved into a big P1 cell (cell dimension $a = b = c = 1{,}000$ Å, $\alpha = \beta = \gamma = 90°$) using the RAVE package of the Uppsala Software Factory (18) to calculate the correlation coefficient at finer grids (24). With the pentamer fivefold axis kept aligned with the icosahedral fivefold axis, the VP1 pentamer was translated along the direction of fivefold axis in 0.1 nm steps from −1.0 to +1.0 nm of the initial position, while at each step it was rotated around the fivefold axis in 1-degree intervals, from 0 to 71 degrees, relative to initial position. During the rigid-body refinement, the

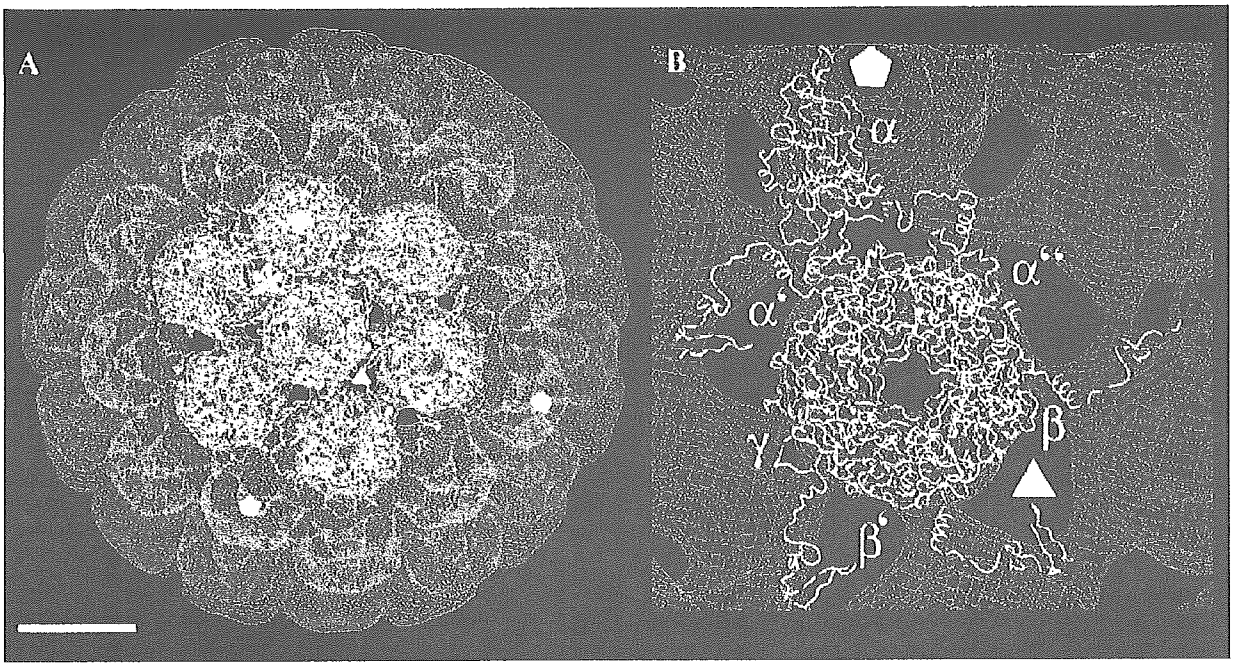

FIG. 5. Fitting of the VP1 model to the density map of the larger $T=7$ particle structure. (A) The density map is viewed along the local sixfold axis, showing the VP1 model fitted to one fivefold pentamer and six local sixfold pentamers. Asterisk, the local threefold position. Bar, 10 nm. (B) Close-up view of the six unique monomers (α, α′, and α″ at the local threefold; β, β′ around the icosahedral threefold; and γ at the twofold). The positions of the threefold and fivefold axes are marked as triangle and pentagons, respectively.

structure of residues 331 to 362 was moved together with the neighboring pentamer. Subsequently, the entire VP1 capsid shell was constructed at each position and orientation according to the icosahedral symmetry. The structure factors were calculated from the models with the B-factor of 100 nm^2 to simulate the resolution limit of the cryo-EM reconstruction map (8, 27), and the correlation coefficient was calculated between the atomic models and the cryo-EM map using CCP4 suite (CCP4, 1994). The pentamer was moved to the position where a maximum correlation coefficient of 0.82 was reached. After the structure that connected the neighboring pentamer was refined, the correlation between the cryo-EM map described above and the final model reached a coefficient of 0.84.

RESULTS

Effect of buffer composition on VLP disassembly and the structure of reassembled particles. The major factors that contributed to the disassembly of $T=7$ VLPs into pentameric capsomers were found to include reduction of disulfide bonds and removal of calcium ions. A combination of a reducing agent and a calcium chelator was required to disassemble the particles. However, dissociation did not occur at very high ionic strength, as seen in the sample treated at ~0.6 M NaCl, in spite of the presence of both reducing agent and EDTA (Fig. 1).

The effect of buffer composition on particle formation from free pentamers was analyzed by dialysis experiments. Samples of free capsomers were exposed to buffers containing different concentrations of $CaCl_2$ and NaCl at various pHs (Fig. 2). Large quantities of small VLPs were formed at low calcium ion concentrations (5 to 10 mM) and in calcium-free buffers. The number of small VLPs decreased when the calcium ion concentration was increased (25 to 100 mM). Although calcium ions were needed to form the $T=7$ VLPs, the number of $T=7$ particles did not change significantly when the calcium ion concentration was increased in the 25 to 100 mM range. At above 300 mM Ca^{2+}, VLP formation was not seen. The concentration of monovalent salt, the pH, or the ionic strength did not directly influence the reassembly of pentamers into higher oligomeric forms.

As mentioned above, a reducing agent was needed to disassemble the BKV VLPs, expressed in insect cells. However, the presence of 2-ME in the reassembly buffer did not prevent the formation of either small or large particles (data not shown).

Three-dimensional reconstruction of the small reassembled BKV VLP. Two BKV VLPs that differed in diameter (26.4 and 50.6 nm) were observed in the low-dose micrograph (Fig. 3). The larger VLPs, with the size of the native virus, were used as an internal reference standard and showed nearly circular image profiles. That indicated that the features of the larger VLPs were well preserved in the vitrified ice. The image profile of the smaller VLPs was also circular, but they did not have the smooth surface of the larger VLPs. Before freezing, the VLP concentration was adjusted so that about 400 particles per micrograph could be selected at the magnification of 45,000.

The structure of the BKV VLP was solved at ~2.4 nm resolution from unstained, frozen-hydrated samples that were imaged with low-irradiation cryo-EM procedures. The three-dimensional reconstruction showed 12 pentameric capsomers in the smaller BKV VLP arranged according to a $T=1$ surface lattice placed on the 12 fivefold rotation axes of the icosahedron (Fig. 4). Due to the smaller diameter of the $T=1$ structure, the unique angle between the capsomers in this particle was 38° greater than that of the average angle between capsomers in the $T=7$ structure (21).

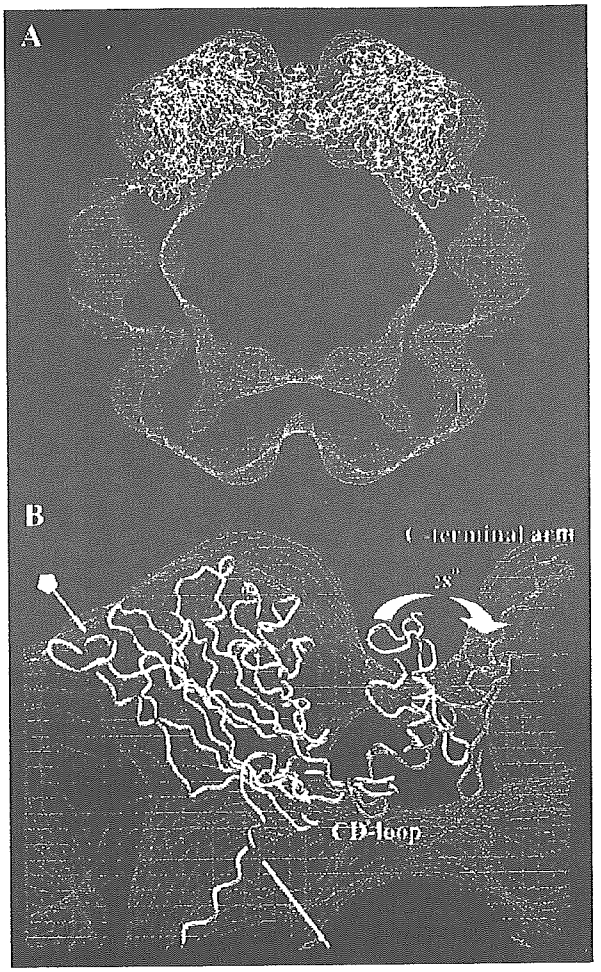

FIG. 6. Fitting of the VP1 model to the density map of the $T=1$ structure. (A) The fivefold monomers from the larger $T=7$ particle were fitted into the density map of the $T=1$ particle. The core of the VP1 model fitted well, while the C-terminal arm was protruding out from the density map at the threefold. This was because the angle between capsomers in the $T=1$ structure was 38 degrees larger than the averaged angle between capsomers in the $T=7$ particle. (B) Parts of two pentamers are seen from the side. There were no structural changes made in the core of the VP1 protein, except for the CD-loop. The unchanged VP1 model is shown in yellow, whereas the modulations made to fit the $T=1$ structure is shown in red. The fivefold axis is marked with a pentagon.

The morphology of the pentameric capsomers was more pronounced in the $T=1$ than in the $T=7$ structure. The $T=1$ capsomers had a diameter of 9.2 nm, which was slightly larger than capsomers in the $T=7$ structure (~1.2 nm larger in diameter). This extra density, compared to the $T=7$ capsomers, was located in the outermost part of each monomer. However, the thickness of the capsid shell was similar, approximately 6.0 nm, in both the $T=1$ and $T=7$ structures.

The major intercapsomeric contact was located at the threefold axis, where the structure protruded from the bottom shell region. The interpentameric contact in the $T=1$ and $T=7$ VLPs at the threefold respective local threefold formed a Y-shaped density connecting three capsomers. This contact remained also when the contour value was raised to 2 sigma (see details in Fig. 7) or following a radial cut of the VLPs capsid shell density. The threefold contact started at a radius of 9.6 nm from the particle center and ended 11.4 nm from the particle center (21.0 to 22.4 nm in the $T=7$ VLP). The density in the twofold axes was much weaker than in the threefold axes. Openings in the capsid shell seen at the threefold and around the twofold axes in the $T=7$ structure were absent in the $T=1$ structure.

Fitting the VP1 model into the density maps of $T=1$ and $T=7$ VLPs. The primary sequence of BKV VP1 has a 74% similarity to the SV40 VP1 that has been solved to a 0.31 nm resolution (34). The similarity is even higher in the C-terminal arm (83%), while the main differences are in the loops at the outer surface of the monomer. A structural model of the BKV VP1 was created by aligning the primary sequence of BKV VP1 with the coordinates of VP1 from SV40 (SV40, PDB: 1SVA). The model of the BKV VP1 was first fit to the density map of the $T=7$ particle to reveal the differences and similarities to particles with the same T-number (Fig. 5A). The only modification required to obtain an excellent fit was an adjustment for the slightly larger radius of the BKV VLP (+0.47 nm of the local sixfold pentamer and +0.58 nm of the fivefold pentamer). The six unique C-terminal arms (α, α', and α'' at the local threefold axis; β, β' around the icosahedral threefold axis; and γ at the twofold axis) (34), responsible for the interpentameric contacts, fitted in the EM density map as well (Fig. 5B).

Each of the six unique monomers was tested as a possible model for the VP1 in the $T=1$ structure. Three of the monomers were excluded because they formed the major interpentameric contact at the twofold axis and had little or no contact at the threefold axis (not shown). In contrast, the three monomers making up the local threefold contact in the $T=7$ structure had their major interpentameric contacts at the threefold axis. The fivefold monomer (α) from the $T=7$ structure was selected as the preferable model of the three, and it was modeled in the density map of the $T=1$ structure.

The core of the VP1 protein (residues 16 to 296) was well fitted to the EM density map (correlation coefficient of 0.82) (Fig. 6A). However, the C-terminal arm protruded out from the density map and did not reach the adjacent capsomer, as the surface curvature was higher within the small-size VLPs compared to the large-size VLPs. Therefore, the angle between the core of VP1 and the outer region of the C-terminal arm required a 28° adjustment in order for the arm to reach the adjacent capsomer (Fig. 6B). The two loops (residues 297 to 300 and 314 to 329) that linked the C-terminal helix to the VP1 protein core and the outermost region of the C-terminal arm were used to increase the angle between the protein core and the C-terminal arm. The last β-strand (the J strand) and the following loop could be modeled in good agreement to the SV40 α monomer. There were, however, additional densities at the side of the monomers. As the structure of the C-terminal domain, covering amino acid residues 348 to 362, had not yet been modeled into the $T=1$ particle, this domain was assumed to account for these additional densities (Fig. 6B).

The structure of the CD loop, which consists of amino acid residues 96 to 106, was rebuilt to that of the α' subunit to avoid a collision with the corresponding loop from an adjacent cap-

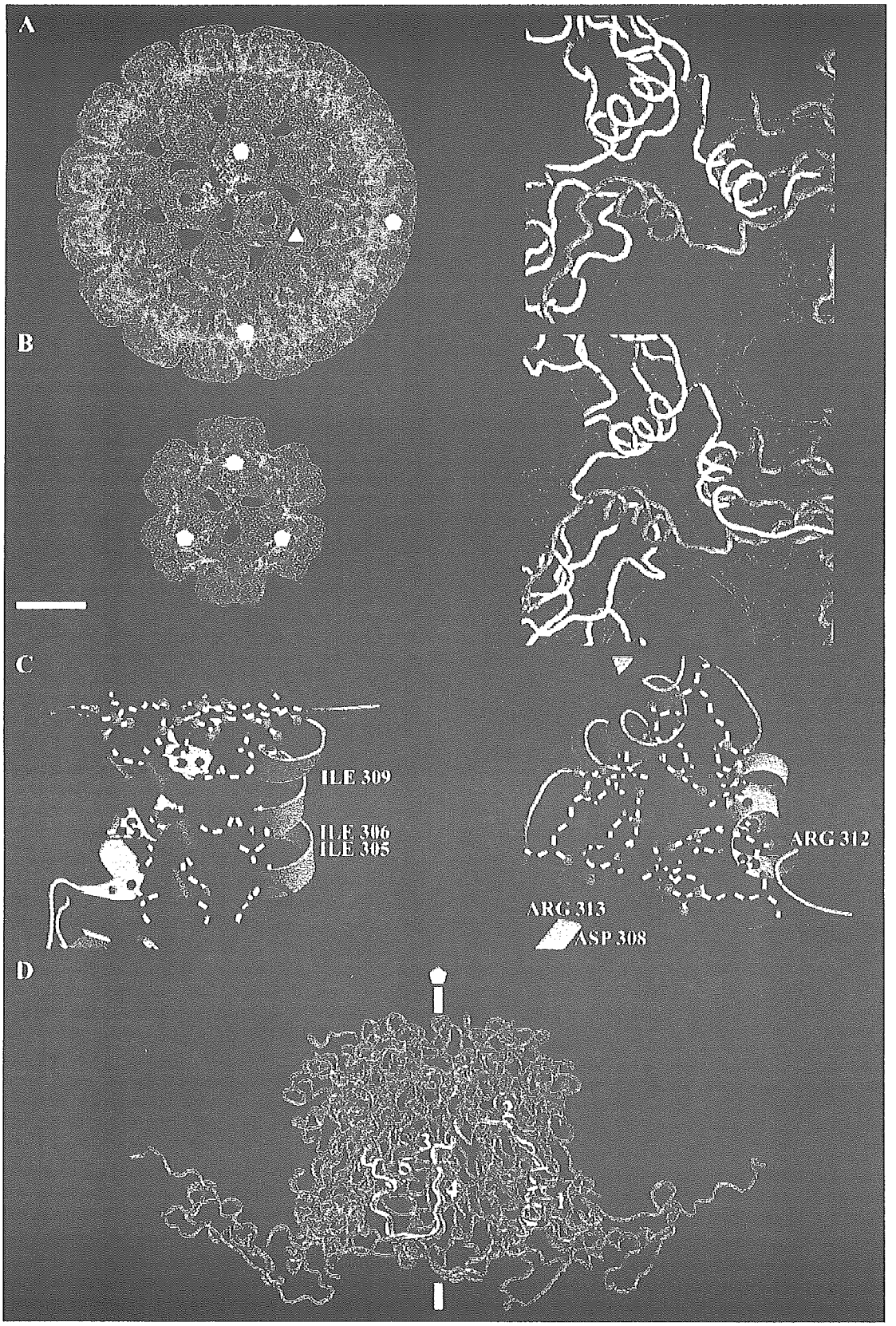
A
B
C
ILE 309
ILE 306
ILE 305
ARG 312
ARG 313
ASP 308
D

somer (34). This region has the highest local root-mean-square deviations between subunits in the $T=7$ particle, suggesting that this region is flexible (Fig. 6B). After refining the C-terminal arm and the CD-loop (the interpentameric connectors), the correlation coefficient between the cryo-EM map, described above, and the final VP1 model reached a value of 0.84.

Interpentameric contacts in the $T=1$ structure. With the adjustments in the C-terminal arm, the structure of a triple-helix bundle, at the threefold axis, was similar to the interpentameric contact at the local threefold axis in the $T=7$ particles (amino acids 300 to 313) (Fig. 7A and B). The three helices were tightly held together by both hydrophobic interactions and salt bridges (Fig. 7C). Furthermore, in the $T=1$ structure the triple-helix bundle was in position to form four hydrogen bonds between each other, which were not seen in the $T=7$ structure. There was, however, a stronger hydrophobic effect within the helix bundle in the $T=7$ structure than in the $T=1$ structure.

To accommodate the higher curvature in the $T=1$ particle than that in the $T=7$ capsid, the C-terminal helix together with the following long loop (amino acids 314 to 329) was tilted 28° away from its own β-barrel core towards the adjacent pentamer. Through this tilt the β-strand J was able to connect with the adjacent pentamer in the $T=1$ structure (Fig. 7D). The long loop, together with the outermost area of the C-terminal arm, composed the region that contributed the least to the interpentameric contact in both the $T=1$ and the $T=7$ capsids. Following the loop, the J-strand made a strong interpentameric contact (with identical interactions as in the $T=7$ structure), starting with one (Glu331) of the two possible calcium-binding amino acids in the C-terminal arm. Amino acid 331 could, however, make an additional salt bridge with amino acid Lys195 in a nearby monomer of the adjacent pentamer. The second amino acid (Asp346) in the C-terminal arm, which was thought to be a calcium-binding site, could establish a salt bridge with amino acid Lys30.

DISCUSSION

The structure of a small VLP of the human BK polyomavirus has been studied and compared with an earlier solved BKV VLP. We have also studied the effect of the buffer composition on VLP disassembly and reassembly processes. The small BKV VLP (26.4 nm in diameter) was shown to have a $T=1$ surface lattice, with a pentamer located at each fivefold axis. In these $T=1$ particles, the main interpentameric contact was found at the icosahedral threefold axis. The angle between the pentamers was 38° greater when compared to the larger BKV VLP (50.6 nm in diameter), which has a capsid composed of 72 pentamers arranged in $T=7$ surface lattices (21). Our observed structure of the $T=1$ particle agrees very well with the computational modeling of the 12-capsomer murine polyomavirus particle done by Salunke et al. (29).

With a 74% similarity to SV40 VP1, the primary sequence of BKV VP1 was aligned with the coordinates of VP1 from SV40 (SV40, PDB:1SVA) to create a structural model of the BKV VP1 (34). This model was first fitted to the density map of the $T=7$ particle in order to reveal the differences and similarities to particles with the same T-number. An excellent fit of the VP1 model to the EM-density map was obtained after an adjustment of the slightly larger diameter of the BKV VLP. The six unique C-terminal arms, responsible for the interpentameric contacts, fitted in the EM density as well.

The fivefold monomer from the $T=7$ structure inserted well into the $T=1$ EM density following an adjustment to particle curvature in the hinge regions of the C-terminal arm. In $T=1$ particles, the pentamers were connected to each other at the icosahedral threefold axis in a similar way as at the local threefold axis in the $T=7$ particle. Here, seen in both particles, the C-terminal arms met in a triple-helix bundle (residues 301 to 313). In the $T=1$ particles this bundle appears to have four additional hydrogen bonds and to be less hydrophobic compared to the $T=7$ structure.

While the outermost part of the C-terminal arm (amino acids 350 to 362) appear to be the most flexible part that do not significantly contribute to the stability of either the small or large VLP, the interactions involving the J-strand is conserved. Thus, the key feature of the capsomer-intervening C-terminal arm is the ability to adjust to the pentamer's relative orientation and particle curvature. In the $T=1$ particle the essential adopting regions are the hinges on both side of the short C-terminal helix. The flexibility in these regions allows the J-strand to insert in the conserved orientation and the short helices from three capsomers to form a bundle, fitting with the cryo-EM map.

A similar type of flexible adaptation in the C-terminal arms has been reported for the $T=1$ and $T=7$ VLPs of the papilloma virus (7, 23). Despite lacking significant sequence similarity, the BKV VP1 (362 residues) and the human papilloma virus 16 L1 (531 residues) both form pentameric capsomers and similar architectures. Also, in the papilloma virus $T=7$ structure the C-terminal arm "invades" adjacent pentamers, keeping the shell together. However, in the $T=1$ structure the C-terminal arms exit the monomer to form the interpentameric contact at the threefold axis and then reinsert into the same monomer,

FIG. 7. Interpentameric interactions in the $T=1$ and $T=7$ BKV VLP. (A) Left: VP1 model of the α (yellow), α′ (red), and α′ (green) monomer fitted to the density map of the $T=7$ particle at the local threefold. Right: close-up of the interpentameric contact "triple-helix bundle" at the local threefold. (B) Left: three $T=1$ VP1 models fitted to the density map of the $T=1$ particle, the particle is viewed along the threefold axis. Right: close-up of the interpentameric contact found at the threefold axis in the $T=1$ particle. (C) Close-up of the triple-helix bundle in the smaller $T=1$ particle, showing possible salt-bridges and hydrophobic interactions. Right, side view; left, top view. (D) The C-terminal arm from the $T=1$ particle (red) and the α monomer from the $T=7$ particle (yellow) are here superimposed to compare interpentameric interactions. The C-terminal arms interact with two monomers in the neighboring pentamer (blue). The C-terminal arms start with a helix at the threefold (in the $T=1$ particle) and at the local threefold in the $T=7$ particle (1). The helix is connected through a long loop (2) to the J-strand (4). The two possible calcium-binding amino acids in the C-terminal arm are also marked, Glu331 (3) and Asp346 (5). The threefold and fivefold are marked as triangle and pentagons, respectively. Bar, 10 nm.